Assimilation of ASCAT Soil Moisture and SMAP Brightness Temperature Observations into the NASA GEOS Land Data Assimilation System

Andrew M. Fox[1,2], Rolf H. Reichle[1], and Qing Liu[1,3]

1. Global Modeling and Assimilation Office (Code 610.1), NASA GSFC, Greenbelt, MD, USA

2. GESTAR-II, Morgan State University, Baltimore, MD, USA

3. Science Systems and Applications, Inc., Lanham, MD, USA

Corresponding Author: Andrew M. Fox (andrew.fox@nasa.gov)

ABSTRACT

Soil moisture (SM) observations from the Advanced Scatterometer (ASCAT) satellite radar (5.3 GHz) and brightness temperature (Tb) observations from the Soil Moisture Active Passive (SMAP) satellite radiometer (1.4 GHz) are assimilated in the NASA Goddard Earth Observing System (GEOS) land data assimilation system, both separately and together (jointly) from April 2015 to March 2021. The resulting SM estimates are validated using in-situ measurements, independent satellite observations, and data assimilation diagnostics. Assimilating only ASCAT SM (ASC_DA) universally improves the SM analysis estimates relative to a model-only control simulation (CNTL). For example, the anomaly time series correlation coefficient (anomR) vs. in-situ surface SM increases from 0.55 for CNTL to 0.58 for ASC_DA, and the misfit between SMAP Tb observations (not assimilated) and corresponding (3-hour) background forecasts decreases by 4.9%. Assimilating only SMAP Tb (SMP_DA) yields greater improvements in SM analysis estimates than does ASC_DA. For example, anomR vs. in-situ surface SM increases to 0.68, although the misfit between ASCAT SM observations (not assimilated) and corresponding (3-hour) background forecasts decreases by only 1.5%. Jointly assimilating multi-sensor (ASCAT and SMAP) observations (MLT_DA) yields overall SM estimation skill similar to that of SMP_DA. Data assimilation diagnostics suggest that MLT_DA background forecasts are generally improved vs. those of CNTL, but by less than seen in SMP_DA, implying that information from the ASCAT and SMAP observations does not always agree. However, since ASC_DA clearly improves SM estimates, multi-sensor assimilation is nevertheless beneficial by increasing system robustness and extending the period when SM observations are available for assimilation.

SIGNIFICANCE STATEMENT

Knowledge of soil moisture—past, present, and future—is crucial for various scientific research areas and practical applications, such as land-atmosphere interactions, drought monitoring, streamflow forecasting, plant productivity, and numerical weather prediction. The best soil moisture estimates are likely obtained by merging data from multiple satellite sensors into numerical land surface models, especially when these sensors provide measurements from different times and locations and use complementary remote sensing techniques. Multiple validation approaches revealed that integrating ASCAT soil wetness observations enhances soil moisture estimates beyond model-only simulations, and using

SMAP brightness temperature further improves these estimates. However, combining both ASCAT and SMAP observations does not yield better results than using SMAP alone. Nevertheless, since using ASCAT clearly improves soil moisture estimates, an approach that uses both types of observations is beneficial, as it increases system robustness and extends the period over which observations are available to improve model estimates.

1. Introduction

Soil moisture is an essential climate variable (Bojinski et al., 2014; Seneviratne et al., 2010). It links the global water, energy and carbon cycles and influences many land surface processes such as runoff and infiltration, the energy partitioning between the latent and sensible heat fluxes, and the transpiration and photosynthesis of plants. Knowledge of past, current, and future soil moisture conditions informs numerous topics of scientific research and applications, including land-atmosphere interactions, drought monitoring, streamflow, biogeochemistry, and numerical weather prediction (Balsamo et al., 2018; Carrera et al., 2019; Crow et al., 2022; De Lannoy et al., 2022; Dong et al., 2022; Guo et al., 2012; Humphrey et al., 2021; Koster et al., 2004, 2016; Reichle et al., 2023b; Santanello et al., 2018; Zhou et al., 2021).

Soil moisture conditions can be inferred from in-situ measurements, remote sensing observations from spaceborne radars and radiometers, or land surface models. In-situ measurements are the most accurate (Kumar et al., 2018) but have very limited spatial coverage. Satellite soil moisture observations provide near-global coverage, but with incomplete temporal coverage due to long revisit times. Satellite observations are also limited to directly sensing only shallow, near-surface soil conditions and rely on complex retrieval algorithms that can result in potentially large uncertainties (Gruber et al., 2020). Land model estimates of soil moisture are spatially and temporally complete but can contain large uncertainties stemming from errors in land model parameterizations or meteorological forcing inputs. Land data assimilation systems can be used to combine the valuable information from remote sensing observations when and where they are available with the process knowledge encoded in land models. The analysis produced by the assimilation thus encapsulates the combined information from the model and the observations and has complete temporal and spatial coverage, including soil moisture estimates through the full

depth of the soil profile (Reichle, 2008). The best estimates of soil moisture will likely be achieved if observations from multiple satellite sensors are assimilated together (jointly), especially if they have different spatial and temporal support and are based on complementary measurement principles (Draper et al., 2012; Lievens et al., 2017; Seo et al., 2021).

Several satellite sensors have been used to retrieve surface soil moisture estimates based on measuring soil dielectric properties. These include the Advanced Microwave Scanning Radiometer for the Earth Observing System (AMSR-E) and its successor, AMSR2, with channels operating at 6.9 GHz and 10.7 GHz (Njoku et al., 2003; Owe et al., 2008; Parinussa et al., 2015) and the radiometer onboard the Tropical Rainfall Measuring Mission (TRMM; Gao et al., 2006) operating at 10.65 GHz. The Advanced Scatterometer (ASCAT; Bartalis et al., 2007; Wagner et al., 2013) measures radar backscatter at 5.3 GHz. These sensors, however, were not primarily designed for observing soil moisture, and their microwave frequencies have a limited soil sensing depth of approximately 1-2 cm. The Soil Moisture and Ocean Salinity (SMOS; Kerr et al., 2010) mission and the Soil Moisture Active Passive (SMAP; Entekhabi et al., 2010a) mission were specifically designed to measure soil moisture; they operate at L-band (1.4 GHz) and have a somewhat greater soil sensing depth of ~5 cm.

Data assimilation systems that use satellite soil moisture observations typically employ simplified or ensemble filtering methods in their land analysis. Both the European Center for Medium-Range Weather Forecasting and the United Kingdom Met Office assimilate ASCAT soil moisture observations using a simplified extended Kalman filter in their operational global weather analysis and prediction systems (De Rosnay et al., 2013; Gómez et al., 2020). Within the NASA Goddard Earth Observing System (GEOS) modeling and assimilation framework, a weakly-coupled data assimilation system for land analysis has recently been developed (Reichle et al., 2021b). The system uses an ensemble Kalman filter (EnKF) to assimilate SMAP brightness temperature (Tb) observations, which was found to improve forecasts of 2 m air temperature and humidity at lead times out to 5 days (Reichle et al., 2023b).

The GEOS land data assimilation system (LDAS; Reichle et al., 2002, 2008) is built around the NASA Catchment Land Surface Model (CLSM; Koster et al., 2000). In its offline (land-only) configuration (i.e., without feedback to the atmosphere), GEOS LDAS has been

used to assimilate a variety of land surface observations, including SMAP Tb (Reichle et al., 2017b), SMOS Tb (De Lannoy & Reichle, 2016a), land surface temperature (Reichle et al., 2010), and terrestrial water storage (Girotto et al., 2016). Other offline systems that assimilate satellite soil moisture observations include the NASA Land Information System (Kumar et al., 2008), the Canadian Land Data Assimilation System (Carrera et al., 2015) and the Community Land Model-Data Assimilation Research Testbed (Zhao et al., 2016).

GEOS LDAS is used to generate the operational SMAP Level 4 Soil Moisture (L4_SM) product, which provides global, 9 km resolution, 3 hourly surface (0 – 5 cm) and root-zone (0 – 100 cm) soil moisture with a mean latency of 2.5 days (Reichle et al., 2019). The L4_SM product has been thoroughly validated by its algorithm development team and independent researchers (e.g. Beck et al., 2021; Colliander et al., 2022; Ford & Quiring, 2019; Pablos et al., 2018; Qiu et al., 2021; Reichle et al., 2017a; Reichle et al., 2017b; Reichle et al., 2023a; Stillman & Zeng, 2018) and was found to be suitable for use in a wide variety of research and applications.

In the present paper, we examine the separate and joint assimilation of ASCAT soil moisture and SMAP Tb observations in a system that is largely equivalent to the operational L4_SM algorithm. Previous studies have jointly assimilated observations from multiple sensors to produce a soil moisture analysis. Using an early version of GEOS LDAS, Draper et al., (2012) found that separately assimilating AMSR-E and ASCAT soil moisture observations gave similar skill improvements, while assimilating them jointly resulted in overall better soil moisture estimates. Moreover, Lievens et al., (2017) examined the assimilation of SMAP Tb and Sentinel-1 synthetic aperture radar backscatter observations; they found that in single-sensor experiments the assimilation of SMAP observations consistently improved estimates of surface and root-zone soil moisture, while the assimilation of Sentinel-1 observations improved only surface soil moisture. The joint assimilation of both types of observations performed best, demonstrating the complementary value of radar and radiometer observations. Finally, Seo et al., (2021) assimilated SMAP and/or ASCAT soil moisture observations into the Joint UK Land Environment Simulator land model across the continental United States. They found that the single-sensor SMAP experiment resulted in the best soil moisture estimates; the average anomaly correlation skill of surface soil moisture increased by 0.05 relative to that of the model-only simulation, while only increasing by 0.01 for the ASCAT experiment. The joint assimilation of soil moisture observations from both

sensors resulted in a skill increase of 0.04, which is comparable to that of the SMAP-only experiment, suggesting that assimilating additional observations of lower quality may have little impact.

As noted above, assimilating SMAP Tb has been found to produce generally better soil moisture estimates than assimilating other observations. Nevertheless, extending the GEOS LDAS to additionally assimilate ASCAT soil moisture observations offers potential benefits. First, the ASCAT record extends back to May 2007, which is nearly 8 years earlier than SMAP, thereby greatly extending the period over which soil moisture observations are available for use in future weather and climate reanalysis efforts. Second, ASCAT's key role in weather analysis and forecasting means that observations are routinely available in near-real time and should remain available at least into the 2040s. That is, adding ASCAT observations to a data assimilation system that assimilates SMAP observations will enhance the robustness of the system, should SMAP become unavailable, if only temporarily, for any reason.

To assess whether these potential benefits can be realized, our study carefully assesses the impact of jointly assimilating ASCAT and SMAP versus assimilating them separately. We employ multiple validation techniques to determine whether the information from the two different types of observations provides complementary, redundant, or potentially contradictory information. We also examine how the number of observations, the effectiveness of bias correction, and observational uncertainty interact to influence the quality of the land surface analysis. In doing so, our study directly addresses key challenges in land data assimilation, including targeted DA, which determines which observations provide the most skill improvement, and multi-sensor DA, which aims to assess whether assimilating different observation types enhances or degrades analysis accuracy (De Lannoy et al., 2022). By rigorously analyzing observation impacts, our study represents a step toward developing a comprehensive land surface reanalysis system that assimilates multiple observation types for improved long-term quality and consistency of future GEOS reanalysis products and predictive capabilities of the GEOS global weather analysis and forecasting system.

The paper is organized as follows: CLSM and the radiative transfer model used to simulate soil moisture and brightness temperature, respectively, along with the ASCAT, SMAP and in-situ observations are described in section 2. The data assimilation system and

our validation approach are outlined in section 3. Results are presented and discussed in section 4. Finally, section 5 provides a summary and suggestions for future work.

2. Model and Data

2.1 Catchment land surface model

CLSM simulates the vertical profile of soil moisture in each of its computational units (Koster et al., 2000). The vertical soil moisture profile is determined by the equilibrium profile, which balances gravity and capillary forces from the surface to the (time-varying) water table, and by deviations from this equilibrium profile in the 0-100 cm "root-zone" layer and the 0-5 cm surface layer. The model prognostic variables for soil moisture are the "catchment deficit" (catdef), "root-zone excess" (rzexc), and "surface excess" (srfexc), from which the volumetric root-zone soil moisture content (0–100 cm) and surface soil moisture content (0–5 cm) are diagnosed, along with the fractions of the saturated, unsaturated, and wilting areas within each computational unit. In the absence of snow cover, the surface temperature is determined by the area-weighted average of the surface temperatures in the saturated (tc1), unsaturated (tc2), and wilting (tc4) areas. Finally, the soil temperature in the uppermost layer (tp1) of the ground heat diffusion module is diagnosed from the model prognostic ground heat content (ght1).

A microwave radiative transfer model coupled to CLSM provides estimates of L-band brightness temperature from the simulated surface soil moisture and soil temperature. In this study, we use a zero-order "tau-omega" model (De Lannoy et al., 2014; De Lannoy et al., 2013). The tau-omega model parameterizations and parameters match those of the L4_SM Version 7 product (Reichle et al. 2023a), except that we use the refractive mixing dielectric model for the soil of Mironov et al. (2004) and applied minor changes to the rough surface reflectivity calculation (including polarization mixing) to match the tau-omega model configuration of the SMAP radiometer soil moisture retrieval algorithm. The updated model resulted in better performance during ongoing algorithm development (not shown) and will be incorporated in the forthcoming Version 8 of the L4_SM product.

2.2 ASCAT soil moisture observations

Soil wetness retrievals derived from C-Band (5.3 GHz) radar backscatter measurements are available from the ASCAT sensors onboard the Meteorological Operational (METOP) series of satellites (Bartalis et al., 2007, 2008; Wagner et al., 2013). Specifically, we assimilate data from METOP-A (May 2007 – November 2021), METOP-B (September 2012 - present) and METOP-C (November 2018 - present) on a swath-based 25 km grid, which are available in BUFR format in near-real time from the European Organisation for the Exploitation of Meteorological Satellites (http://h-saf.eumetsat.int) (Collection ID EO:EUM:DAT:METOP:SOMO25). Relative wetness (or surface degree of saturation) in the upper 0-2 cm soil layer is retrieved by applying a change detection algorithm (Naeimi et al., 2009; Wagner et al., 1999) to the ASCAT backscatter time series. The soil wetness retrievals range between 0% and 100% in relative saturation units, with the 0% and 100% values representing the driest and wettest observations at each location, respectively. The bias correction applied to the ASCAT observations (section 3.2) implicitly converts their native relative wetness units into volumetric soil moisture units ($m^3\,m^{-3}$); hereinafter, we use the term "ASCAT SM" when referring to the ASCAT observations after the bias correction has been applied. The bias correction further ensures that the assimilated ASCAT SM observations remain bounded (section 3.2). Being bounded, ASCAT SM observations cannot be strictly Gaussian. Nonetheless, past work suggests that the EnKF is adequate for soil moisture data assimilation despite such non-Gaussianity (Dibia et al., 2023).

Prior to bias correction and assimilation, ASCAT soil wetness retrievals with adverse quality control (QC) flags are removed. Specifically, we remove soil wetness retrievals when any bit in the "processing flag" is set, when any bit in the "correction flag" is set (with the exception of bit 3, which indicates that a correction of wet backscatter was applied; Bartalis et al., 2008), when the "land fraction" is less than 90%, or when the "topographic complexity" or "inundation fraction" are greater than 10%. In addition to using the QC flags available for each observation, we also apply a fixed spatial mask to remove retrievals potentially impacted by subsurface scattering, as recommended by the ASCAT product developers (Wagner et al., 2024). Finally, retrievals are also excluded when and where CLSM indicates frozen or snow-covered ground.

A differently packaged ASCAT soil wetness retrieval product is used for validation (see section 3.4.2). Specifically, we used the inter-satellite calibrated surface soil moisture climate data record (CDR) version 7 (H SAF, 2021a) and its version 7 extension (H SAF, 2021b).

This product provides SM time series for individual grid cells, which is more convenient for validation purposes. The QC for the ASCAT CDR followed the procedures outlined in (Reichle et al., 2021a). Specifically, we included only retrievals with a favorable surface state flag (SSF=1) and a favorable confidence flag (CONF_FLAG=0). Additional QC measures were applied based on the consistency between the satellite and model estimates (see section 3.4.2 for details).

2.3 SMAP brightness temperature and soil moisture observations

The SMAP satellite is equipped with an L-band radiometer that is highly sensitive to water in the surface (0-5 cm) soil layer and the vegetation (Entekhabi et al., 2010a; Jackson & Schmugge, 1991; Schmugge et al., 1974). SMAP collects observations of horizontal (H) and vertical (V) polarization brightness temperatures (Tb) from a sun-synchronous, near-circular, polar orbit with equator crossings at 6 AM and 6 PM local time and a revisit time of 2-3 days. Here we assimilate forward- and aft-looking SMAP Level 1C Tb observations (Chan et al., 2023) in both H- and V-polarization and from both the AM and PM overpasses. The observations are provided on the 36-km resolution Equal-Area Scalable Earth version 2 (EASEv2) grid (Brodzik et al., 2012). A SMAP Tb observation was assimilated only if the corresponding bit flag for its overall quality (cell_tb_qual_flag_[h/v]_[fore/aft]) was not set.

We also use SMAP surface soil moisture retrievals for validation when SMAP Tb observations were not assimilated (section 3.4.2). Specifically, we used retrievals from the SMAP Level 3 radiometer global daily 36-km EASE-grid soil moisture version 8 product (O'Neill et al., 2021). For quality control, we included only retrievals with a "retrieval succeeded" flag and good "tb quality" flags. Additionally, we excluded retrievals with the "surface flag" indicating "model frozen ground", or "snow and ice". Additional QC was applied for the validation based on the Instrumental Variable approach (see section 3.4.2 for details). Finally, we excluded SMAP Tb observations and SMAP soil moisture retrievals from the assimilation or validation when CLSM indicated that the soil was frozen or snow-covered.

2.4 In-situ soil moisture measurements

Our primary in-situ soil moisture validation dataset is from the SMAP core validation sites (Colliander et al., 2017, 2022). These data are particularly valuable because each core

site has a locally dense network of sensors that ameliorates the typical upscaling errors when comparing in-situ measurements with model grid cell output (Crow et al., 2012).

Across the network, the time-average number of individual surface soil moisture sensors within the 33-km validation grid cells (or "reference pixels") ranges between 6.0 and 28.1, with a mean value of 13.4; the corresponding number of sensor profiles for root-zone soil moisture ranges between 8.9 and 22.8, with a mean value of 15.1 (Reichle et al., 2023a). Moreover, the core site measurements are fully independent of any calibration of CLSM. For calculating our validation statistics, we use surface (root-zone) measurements from 18 (8) different core sites situated in a wide variety of climate regimes and land cover classes (Table S1 in the Supplemental Material). The 6-year period from 1 April 2015, 0z to 1 April 2021, 0z is used for the core site validation because more recent in-situ measurements are available for only a small minority of the sites. In-situ measurements are used for validation only when the model (or assimilation) estimates indicate non-frozen and snow-free conditions. For additional information about the in-situ measurements and validation approach, see Reichle et al. (2017a; their section 3).

3. Assimilation System

3.1 GEOS land data assimilation system

GEOS LDAS couples CLSM with a spatially distributed ensemble Kalman filter (EnKF) that updates the model state based on comparison with relevant observations and accounts for the uncertainties in both the model and the observations. Here, we utilized the system's established assimilation of SMAP Tb observations (section 2.3) and extended it to also assimilate ASCAT SM observations from ascending and descending orbits from METOP-A, -B and -C (section 2.2), either separately or jointly with the SMAP Tb observations.

Like in the L4_SM algorithm, a 24-member ensemble is used to estimate model forecast uncertainty, with ensemble spread maintained by continuously perturbing select CLSM prognostic variables (catdef and srfexc) and meteorological forcings (precipitation, downward shortwave and longwave radiation). The perturbation parameters used here match those of (De Lannoy & Reichle, 2016b) (their Table 2) except that the spatial correlation scale for the perturbations of the model prognostic variables is set to 0.3° and the standard-normal deviates generated for the multiplicative perturbations of the precipitation and

downward shortwave forcing are truncated at ±3. These changes make the perturbation parameters consistent with those of the L4_SM Version 7 product.

We set the SMAP Tb observation error standard deviation to the constant 4 K value of the L4_SM algorithm, which includes an estimated 1.3 K instrument error standard deviation and 3.8 K representativeness error standard deviation (i.e., error in the radiative transfer model and remapping associated with the observation operator) (Gruber & Reichle, 2022; Reichle et al., 2017a), which are added in quadrature. The ASCAT SM observation error standard deviation was set to 9% (in relative saturation units) using previous estimates established using the triple colocation technique (Dorigo et al., 2010). This is converted into volumetric soil moisture units during the bias correction step, based on location-specific soil properties used in CLSM (section 3.2). Based on the rule-of-thumb that a soil moisture change of 0.01 m^3m^{-3} corresponds to a Tb change of ~2-3 K (De Lannoy et al., 2019), and assuming a soil porosity of ~0.5 m^3 m^{-3}, the observation error assigned to ASCAT is at least twice as large (in comparable units) as that ascribed to SMAP.

Every 3 hours (at 0000, 0300, ..., and 2100 UTC), the EnKF analysis uses the available ASCAT SM and/or SMAP Tb observations within the 3-hour window centered on the analysis time and produces increments (or correction terms) for the model prognostic variables associated with the surface and root-zone soil moisture and the surface and top-layer soil temperature. In the case of ASCAT SM observations, the EnKF state vector includes srfexc and rzexc, and additionally catdef for grid cells modeled as peatlands. For SMAP Tb observations, the EnKF state vector includes srfexc and rzexc (and catdef in the case of peatlands) plus the model prognostic variables for surface temperature (tc1, tc2, and tc4) and the layer-1 ground heat content (ght1) (section 2.1). The latter EnKF state vector is also used when ASCAT SM and SMAP Tb observations impact a single model grid cell within the same 3-hour assimilation window.

The magnitude of the analysis increments depends on the misfit between the observed and simulated surface soil moisture (ASCAT) and Tb values (SMAP), that is, the observation-minus-forecast (OmF) residuals (or “innovations”). It further depends on the ensemble-simulated error covariances between the simulated observation-space (soil moisture and Tb) diagnostics and the CLSM prognostics that make up the EnKF state vector. Error covariances between surface and root-zone soil moisture therefore allow updating the latter using observations that are primarily sensitive only to surface-layer conditions.

For both ASCAT SM and SMAP Tb, the OmF residuals used in the EnKF analysis are computed after first removing the seasonally varying ASCAT SM (or SMAP Tb) climatology from the observed values and the corresponding model forecast climatology from the model forecast values (De Lannoy & Reichle, 2016a; section 3.2). Therefore, only the observed *anomalies* from the climatological seasonal cycle are assimilated and, by design, the EnKF analysis does not correct for systematic errors, such as might be found in precipitation forcing (Reichle et al., 2023a). This is because the EnKF assumes unbiased errors; using the EnKF to correct for bias can result in misleading updates and unrealistic state estimates. Finally, the resulting analysis increments are added to the model forecast estimates of the EnKF state and, starting from the corrected model prognostic variables, the simulation continues for three hours until the next analysis time.

The EnKF update is spatially distributed (or 3-dimensional) in the sense that at a given 36 km grid cell, all observations within a radius of 1.25° impact the (surface and root-zone) analysis (De Lannoy & Reichle, 2016a; their section 3.1). The weight contributed by an OmF residual toward the soil moisture (or temperature) increments at a given 36 km grid cell is proportional to the ensemble-estimated forecast error correlations between the ASCAT SM or SMAP Tb observation at the observation location and the soil moisture (or temperature) at the location of the increment. Since this error correlation typically decays with increasing distance of the observation from the location of the increment, its sample-based estimate becomes relatively noisier with increasing distance. This is addressed through a distance-based covariance localization approach with a compact support radius of 1.25° (De Lannoy & Reichle, 2016a; Gaspari & Cohn, 1999), which is the maximum distance over which an observation can have an impact.

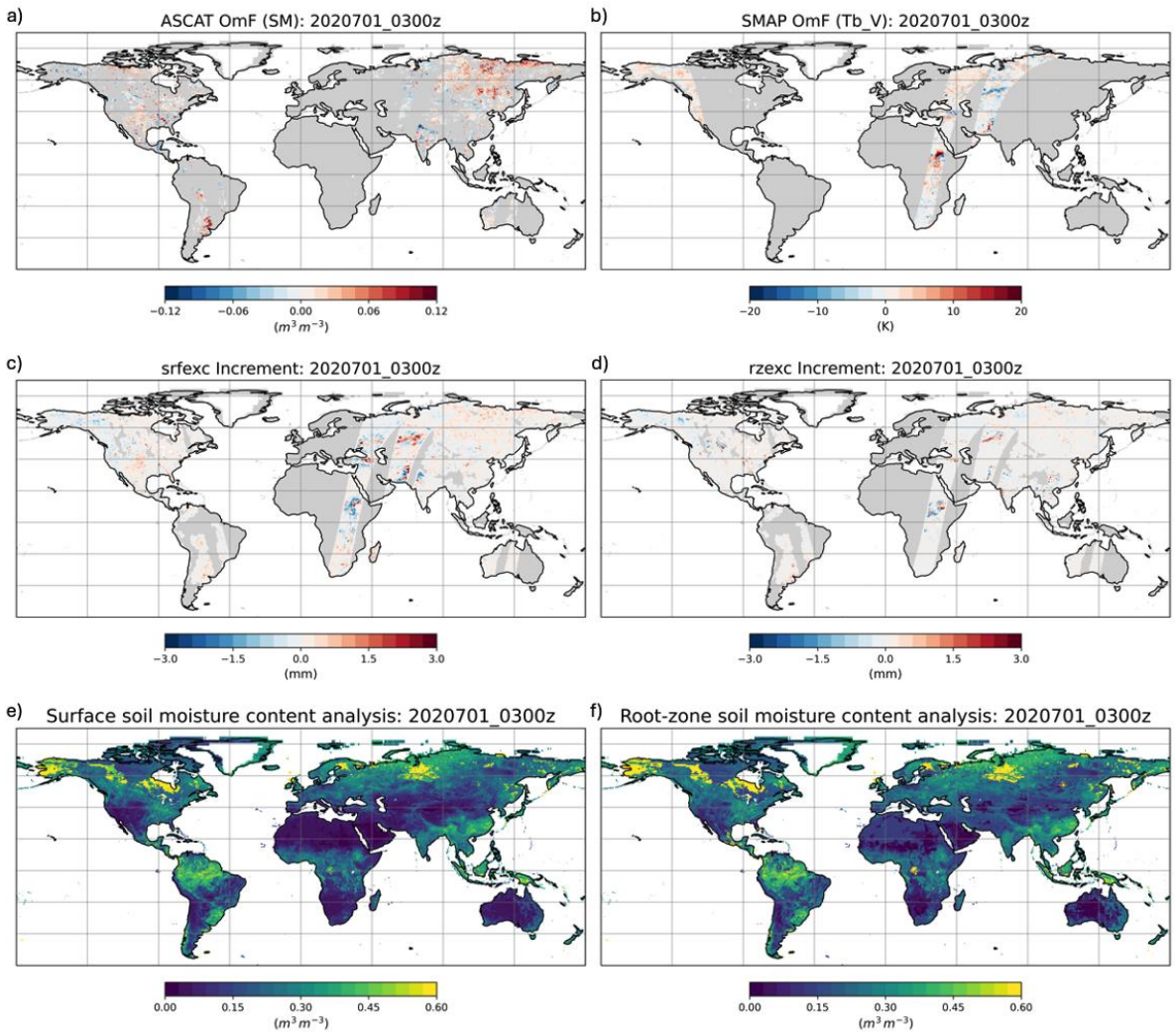

Figure 1. *Illustration of key stages in the soil moisture update in the joint assimilation of ASCAT soil moisture (SM) and SMAP brightness temperature (Tb) on 1 July 2020 at 03:00 UTC. (a) ASCAT SM OmF; (b) SMAP Tb OmF for V-polarization; (c, d) increments in surface excess (srfexc) and root-zone excess (rzexc); (e, f) analysis of surface soil moisture content and root-zone soil moisture content. Grey shading indicates no-data values.*

Figure 1 illustrates the key stages in the soil moisture analysis outlined above for a single 3-hour assimilation window centered on 03:00 UTC on 1 July 2020. Figure 1a-b shows swaths of footprint-scale OmF residuals for ASCAT SM and SMAP V-polarization Tb, respectively. (The corresponding map for H-polarization Tb OmF residuals looks very similar to that for V-polarization; not shown.) The EnKF transforms the OmF residuals into increments in srfexc (Figure 1c) and rzexc (Figure 1d). Positive Tb OmF values indicate that the Tb forecast is too cold, which implies that the soil moisture model forecast is too wet and results in negative (drying) soil water increments. Conversely, positive ASCAT SM OmF

values indicate that the model forecast is too dry, resulting in positive (wetting) soil water increments, and vice versa for OmF residuals with the opposite sign. The increments associated with ASCAT SM observations (e.g., across North America and eastern Siberia) are generally smaller than those associated with SMAP Tb observations (e.g., across eastern and southern Africa and central Asia) (Figure 1c-d), which is consistent with the aforementioned difference in the assigned ASCAT and SMAP observation error standard deviations. The increments are then added to the model forecast values to produce the analysis of surface (Figure 1e) and root-zone (Figure 1f) soil moisture, shown here in volumetric soil moisture units. The analysis estimates are spatially complete and differ from the corresponding forecasts where observations were assimilated (not shown). The corresponding analysis of the model prognostic excess and deficit variables is then used to initiate the next timestep of model integration.

3.2 Bias correction

Bias in modeled soil moisture and Tb is expected, owing to systematic errors in land model parameterizations, parameters, and forcing data. Since the EnKF analysis is not designed to correct for bias, the assimilated observations are scaled to match the climatology of the corresponding model estimates.

Prior to assimilation, we subtract the observed mean seasonal cycle from the SMAP Tb observations and then add the corresponding seasonal cycle of the simulated Tbs (separately for each grid cell). Thus, only the anomaly information contained in the SMAP Tb observations is assimilated.

We apply a Z-score transform to the ASCAT relative wetness observations; that is, we subtract the observed mean seasonal cycle, multiply the resulting anomalies with the ratio of the simulated to the observed temporal standard deviations (computed over the entire experiment period), and then add the mean seasonal cycle of the CLSM-simulated volumetric surface soil moisture estimates. Finally, the scaled ASCAT SM observations are further restricted to fall within the range given by the driest and wettest modeled values sampled over the experiment period (separately for each grid cell). In this case, only the normalized anomaly information contained in the ASCAT relative wetness observations is assimilated. The bias correction also implicitly converts the ASCAT observations from their native relative wetness units (%) to the volumetric soil moisture units ($m^3\ m^{-3}$) of the CLSM volumetric surface soil moisture forecasts. While the physical relationship between ASCAT

relative wetness and volumetric soil moisture is nonlinear, we apply a linear anomaly mapping using a Z-score transform, as it is computationally efficient and consistent with the assumptions of the EnKF, which requires approximately Gaussian errors and linear error propagation.

The seasonal cycles of the mean and standard deviation of the observations and model estimates are computed from the data across the entire experiment period. For this calculation, the simulated data are masked to the times and locations for which good-quality observations are available. The Tb mean seasonal cycles are calculated on the 36-km EASEv2 grid. The ASCAT relative wetness observations, which are provided on a 25-km swath grid, are first binned onto a regular 0.25° latitude/longitude grid, and the seasonal cycle of their mean and standard deviation is calculated on this grid, as is that of the corresponding model forecasts. All seasonal cycles are computed separately for each pentad of the year using a 75-day smoothing window centered on the pentad, provided there are at least 20 (5) good-quality SMAP (ASCAT) observations.

The effectiveness of the bias correction approach applied here is influenced by several factors, including long-term data quality, regional variations, and land cover characteristics. Long-term data quality is important because systematic errors in the observational record, such as sensor degradation, changes in retrieval algorithms, or shifts in calibration standards can introduce inconsistencies over time. If the historical dataset used for determining the bias correction parameters is not stable, the correction may lead to artificial trends or step changes in soil moisture estimates. Moreover, the systematic differences between the model and the observations vary across different regions and land cover types owing to differences in surface characteristics, vegetation density, and climate regimes. To help address these variations, our approach applies a localized and seasonally varying bias correction. However, this approach may still not fully capture short-term variations such as those caused by the harvesting of crops, thereby potentially limiting the effectiveness of data assimilation in highly dynamic environments.

3.3 Experiments

To investigate the impact of assimilating ASCAT SM observations into GEOS LDAS we carried out four experiments (Table 1). All four experiments are identically configured in terms of the model setup, resolution, forcing, ensemble size and perturbations. The experiments differ only in the kinds of observations that are assimilated. For each

experiment, a 24-member CLSM ensemble with perturbations is run on the 36-km EASEv2 grid for 6-years from 1 April 2015 to 31 March 2021, driven with surface meteorological forcing data from the GEOS Forward Processing (FP) system at 0.25° x 0.3125° (latitude x longitude) resolution (Lucchesi, 2013). The CLSM ensemble was spun up for 9 months from 1 July 2014. The ensemble spin-up was initialized from a single-member CLSM simulation spanning the 24.5 years from 1 January 1990 to 1 July 2014 driven with surface meteorological forcing from the Modern-Era Retrospective analysis for Research and Applications version 2 (Gelaro et al., 2017).The GEOS-FP and MERRA-2 precipitation is used here without the daily observations-based corrections of the L4_SM Version 7 product (Reichle et al. 2023a). To ensure climatological consistency across the spin-up and experiment periods, however, the GEOS-FP and MERRA-2 precipitation was rescaled to match the (seasonally-varying) precipitation climatology that is used in the L4_SM Version 7 product.

Experiment Name	**Experiment Description**	**Assimilated Observations**	**Passive Observations**
CNTL	Model-only control simulation	None	ASCAT SM, SMAP Tb
ASC_DA	ASCAT SM data assimilation	ASCAT SM	SMAP Tb
SMP_DA	SMAP Tb data assimilation	SMAP Tb	ASCAT SM
MLT_DA	Multi-sensor data assimilation	ASCAT SM, SMAP Tb	None

Table 1. *Overview of experiments. Passive observations are ingested only to obtain OmF residuals as a diagnostic and do not contribute to the analysis increments.*

The CNTL experiment is a control (or "open-loop") ensemble simulation without any data assimilation. The 24 model ensemble members are forced and perturbed in the same way as in a data assimilation run, and for every three-hour assimilation window, the available (bias-corrected) ASCAT SM and SMAP Tb data are ingested as "passive" observations to produce OmF residuals, which are saved for the purpose of validation (section 3.4.3). That is, in the CNTL experiment, the EnKF is not employed to calculate analysis increments, and the next model integration timestep begins from the previous forecast with no update. The skill of this model-only control run can then be assessed with the validation techniques discussed below (section 3.4) and serves as a baseline for the impact of the satellite data assimilation.

The ASC_DA experiment assimilates only ASCAT SM observations and ingests SMAP Tb data as passive observations. That is, only the misfit between ASCAT SM observations and the corresponding surface soil moisture forecast is used by the EnKF to calculate increments for srfexc and rzexc (and catdef for peatlands), whereas SMAP Tb observations are not used in the calculation of the soil moisture or soil temperature analysis increments. This experiment is designed to test whether ASCAT SM can provide meaningful soil moisture information in the absence of SMAP observations. Demonstrating this capability would enhance system robustness in scenarios where SMAP Tb observations become unavailable; it would also allow for an extension of the observational record to periods before SMAP became operational in 2015.

Conversely, the SMP_DA experiment assimilates only SMAP Tb observations and ingests ASCAT SM data as passive observations. This experiment serves as the DA benchmark, representing our current best system where only SMAP Tb is assimilated to update soil moisture and temperature states.

Finally, the MLT_DA experiment assimilates both ASCAT SM and SMAP Tb, with both types of observations contributing to the soil moisture analysis increments. This experiment assesses whether the combined assimilation of ASCAT and SMAP improves the analysis compared to single-sensor assimilation. It helps identify when and where the integration of both types of observations leads to improvements and under what conditions potential inconsistencies arise, informing the development of more robust multi-sensor data assimilation strategies.

3.4 Validation

3.4.1 IN-SITU VALIDATION

The unbiased root-mean-square difference (ubRSMD, or standard deviation of the error (Entekhabi et al., 2010b)), time series correlation (R), and anomaly R (anomR) metrics versus the in-situ measurements (section 2.4) were computed as in Reichle et al. (2019). For a given site, these metrics are computed from 3-hourly data, provided at least 480 measurements (or about 2 months of data) are available after QC. Calculating anomR requires that there is an estimate of the 6-year mean seasonal cycle. The latter is computed separately for each day of the year using a 31-day smoothing window when there are at least 240 measurements across the 6-year validation period. The mean seasonal cycle of the model or assimilation

experiments is computed after temporal cross-masking with the available in-situ measurements. Summary metrics are calculated by averaging across the metrics from all individual core sites, giving equal weight to each. Statistical uncertainty in the ubRMSD, *R*, and anomR metrics is estimated using 95% confidence intervals, which are computed at each site based on the number of samples in the time series (with a correction for temporal autocorrelation (Dawdy & Matalas, 1964)).

3.4.2 Instrumental Variable approach

Differences in soil moisture anomR skill between the experiments is additionally quantified using independent satellite soil moisture observations when available, following the "single" Instrumental Variable (IV) approach of Su et al. (2014). Briefly, the IV method obtains the difference in skill between two sets of surface soil moisture estimates – in this case the CNTL experiment and either ASC_DA or SMP_DA – versus an unknown true soil moisture through their sample anomaly correlation versus independent satellite observations. By leveraging the temporal persistence of soil moisture, we use a lagged satellite dataset as an instrument to correct for bias in the estimated anomR metric. This approach is analogous to Two-Stage Least Squares regression, where the instrumental variable helps isolate the true relationship between variables by removing endogeneity or measurement error (Wooldridge, 2024). Reichle et al. (2021a; their Fig. 4) successfully verified ASCAT SM-based IV metrics for a SMAP Tb assimilation experiment against metrics derived from in-situ measurements at the above-mentioned SMAP core validation sites. A more detailed discussion of the IV method, including key equations, is provided in section S2 of the Supplementary Material.

Here, SMAP Level 3 soil moisture is used as the IV to assess the single-sensor ASCAT assimilation (ASC_DA), and ASCAT relative wetness is used as the IV to assess the single-sensor SMAP assimilation (SMP_DA), thereby ensuring independence between the assimilation system and the validation data. Since MLT_DA assimilates both ASCAT and SMAP observations, it is not validated using the IV approach for lack of independent observations. (Note that SMOS soil moisture retrievals and the assimilation of SMAP Tb observations in GEOS LDAS both rely on similar L-band radiative transfer modeling and are not independent.)

In addition to the QC applied to the satellite observations outlined in sections 2.2 and 2.3, for the IV-based validation we applied additional QC based on consistency metrics between the satellite and model soil moisture (Reichle et al., 2021a). As part of this additional QC, we

excluded locations where the IV-based estimate of soil moisture anomR skill fell below 0.1 for any satellite-experiment pair. This threshold helps ensure that the independent data have sufficient skill to act as a valid instrument, because statistical error estimators can become unstable with low-quality inputs (Dong et al., 2018). A 0.1 inter-product correlation coefficient is commonly adopted as a lower bound for meaningful analysis (e.g., Dong et al., 2020). Moreover, locations where the soil moisture anomalies from the satellite product and the assimilation experiment had a negative pairwise cross-correlation or 2-day lagged autocorrelation were also excluded. Finally, note that in the present paper we focus exclusively on differences in skill metrics, which mitigates potential issues with bias in the absolute skill metrics derived from the IV method.

3.4.3 Data assimilation diagnostics

All data assimilation systems, including GEOS LDAS, produce internal diagnostics that can be used to assess whether the system is performing well and as expected. The statistics of the OmF residuals and soil moisture analysis increments are typically the most informative metrics. A detailed description of their use in the evaluation of the L4_SM product can be found in Reichle et al. (2017b; their section 2c). It is important to keep in mind that OmF residuals for ASCAT observations are in the units of the scaled ASCAT SM observations, that is $m^3\ m^{-3}$ (section 3.2). Similarly, Tb OmF residuals are in brightness temperatures units (K). As higher soil moisture and lower Tb both indicate wetter soils, the sign of the OmF residuals will be opposite when the forecast is too wet relative to observations (negative OmF for soil moisture and positive OmF for Tb), and vice versa. OmF residuals will always be at the spatial resolution of the observations, although for time series statistical analysis and plotting, each observation is assigned to the closest model grid cell. The soil moisture analysis increments, on the other hand, will have the same units as the incremented "excess" and "deficit" model variables ($kg\ m^{-2}$, equivalent to mm) and be at the model grid cell resolution.

Much of the value in the OmF residuals comes from the fact that each OmF value is calculated *before* the observation is assimilated. In other words, the observations used in the OmF residuals provide independent information in the evaluation of the model forecast. If the assimilation system is performing well and the observations have been bias-corrected, the long-term mean of the OmF residuals should be close to zero, indicating there is no net addition or subtraction of water. Therefore, from a diagnostics perspective, the time series

standard deviation of the OmF residuals is more informative than their long-term mean. The OmF standard deviation provides an estimate of the typical misfit between the model forecast and the (scaled) observations, which can be used to estimate how "hard" the assimilation system is working to correct model states. A reduction in the time series standard deviation of the OmF residuals indicates that the assimilation improved the model forecasts. For this reason, we also examine the time series standard deviation of the analysis increments.

Unlike the assimilated observations, the model forecast and the analysis are always spatially complete across the model domain (Figure 1). For any given 3-hour analysis window, the increments therefore trivially vanish across much of the global domain simply because no observations were assimilated within the 1.25° compact support radius (section 3.1). To exclude these trivially vanishing increments, we consider only soil moisture increments with an absolute value greater than 0.0002 $m^3\ m^{-3}$ in the calculation of the statistics. This threshold is required because the volumetric soil moisture increments are computed here as the difference between the analysis and forecast fields, which entails roundoff error and prevents us from identifying exact zeros. As a side effect, this approach excludes the presumably rare increments that are very small because the model forecast and the observations agreed closely. We verified that our results are not sensitive to the exact value of the applied threshold.

4. Results and Discussion

4.1 In-situ metrics

The summary performance metrics across the SMAP core validation sites are shown in Figure 2. The performance metrics for the CNTL experiment provide a baseline for CLSM's ability to simulate surface and root-zone soil moisture when driven with GEOS-FP surface meteorological forcing. The *R* and anomR values for CNTL range between 0.55 and 0.67, and the ubRMSD for CNTL is 0.042 $m^3\ m^{-3}$ for surface soil moisture and 0.031 $m^3\ m^{-3}$ for root-zone soil moisture, indicating that CLSM driven with GEOS-FP precipitation has reasonable skill in simulating soil moisture, but that there is also room for improvement through assimilating soil moisture observations.

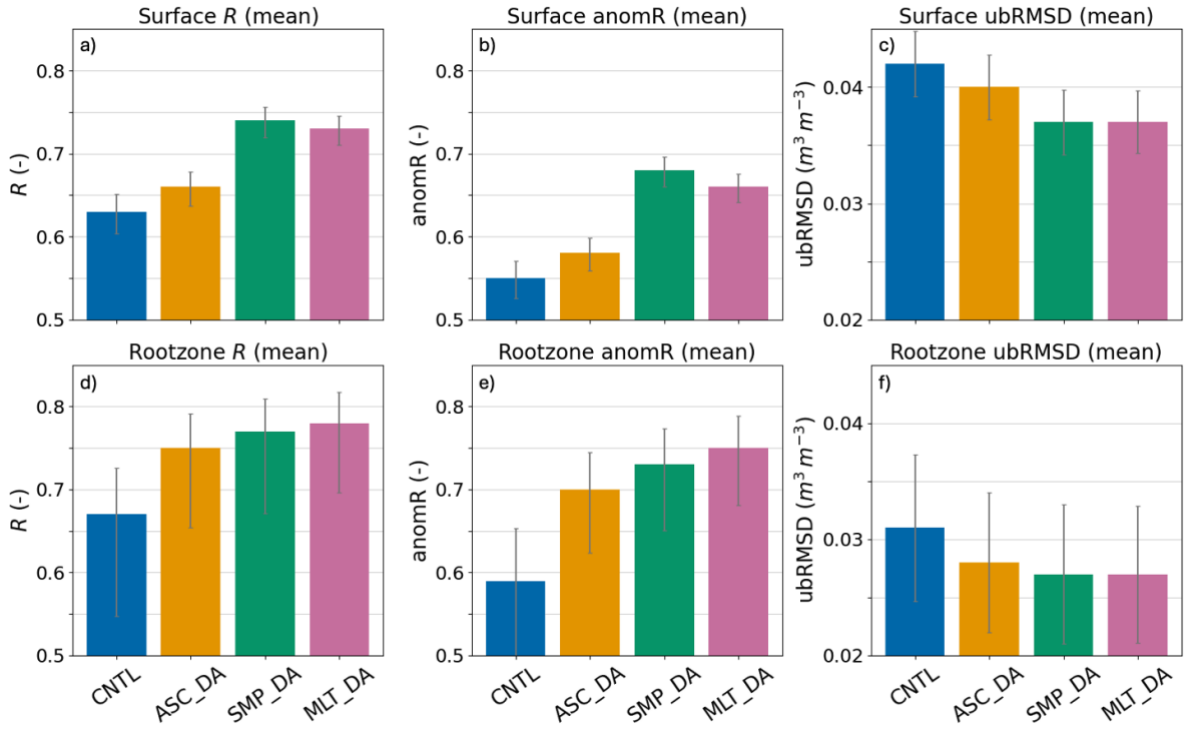

Figure 2. *Performance metrics vs. in-situ measurements for (a-c) surface soil moisture at 18 SMAP core validation sites and (d-f) root-zone soil moisture at 8 sites. Metrics include (a,d) time series correlation (R), (b,e) anomaly R (anomR) and, (c,f) unbiased root mean square difference (ubRMSD).*

Assimilating only ASCAT SM observations in the ASC_DA experiment yields small but consistent improvements in all metrics for surface and root-zone soil moisture skill relative to the CNTL experiment. While these skill differences are not statistically significant for any single metric, as indicated by the overlapping 95% confidence intervals, their consistency across several metrics suggests an overall beneficial impact from the assimilation of ASCAT observations. For surface soil moisture, *R* increases from 0.63 for CNTL to 0.66 for ASC_DA, anomR increases from 0.55 to 0.58, and ubRMSD decreases from 0.042 to 0.040 m^3 m^{-3}. The equivalent differences are relatively larger for root-zone soil moisture, with *R* increasing from 0.67 for CNTL to 0.75 for ASC_DA, anomR from 0.59 to 0.70, and ubRMSD decreasing from 0.031 to 0.027 m^3 m^{-3}. This overall improvement is a reassuring result, indicating that the ASCAT observations contain useful information about surface soil moisture. Moreover, the results suggest that GEOS LDAS can effectively incorporate ASCAT data to improve CLSM soil moisture estimates across the range of land cover types and environmental conditions represented by the SMAP core validation sites.

When only SMAP Tb observations are assimilated (SMP_DA), the improvements vs. CNTL are larger across all skill metrics compared to those achieved with ASC_DA. For SMP_DA, the *R* and anomR metrics for surface soil moisture (Figure 2a, b) show statistically significant improvements vs. CNTL (and vs. ASC_DA), with *R* increasing from 0.63 for CNTL to 0.74 for SMP_DA and anomR increasing from 0.58 for CNTL to 0.68 for SMP_DA. This result is consistent with the long history of validation results for the L4_SM product (e.g. Beck et al., 2021; Colliander et al., 2022; Qiu et al., 2021; Reichle et al., 2017a; Reichle et al., 2017b) and with the L4_SM product's emphasis on improving correlation skill. It also backs the assertion that SMAP Tb observations contain more information about the true surface soil moisture state than do ASCAT SM observations. Other studies have come to similar conclusions. For example, using triple co-location-estimated correlation metrics Chen et al. (2018) confirmed the overall advantage of SMAP (with a global average anomaly correlation of 0.76) over SMOS (0.66) and ASCAT (0.63). Using information theory-based metrics Kumar et al. (2018) found the information content of soil moisture products derived from AMSR-E, ASCAT, SMOS and AMSR2 to be lower than that of the SMAP product. Finally, Al-Yaari et al. (2019) found better performance, particularly in terms of temporal dynamics, for SMAP and SMOS than for ASCAT when validating against in-situ soil moisture measurements from the International Soil Moisture Network (Dorigo et al., 2021). Finally, note that the SMP_DA skill metrics reported here are slightly worse than those for the L4_SM product (Reichle et al., 2023a) because the L4_SM algorithm additionally uses observation-based precipitation to drive CLSM, which is not used in this study to isolate the impact of assimilating the different observation types.

The joint assimilation of ASCAT SM and SMAP Tb observations, experiment MLT_DA, gives results that are very similar to those of SMP_DA. The ubRMSD metrics for the two experiments are nearly identical. While the *R* and anomR metrics are slightly better in MLT_DA than in SMP_DA for root-zone soil moisture, the reverse is true for surface soil moisture. The statistical indistinguishability of MLT_DA and SMP_DA indicates that while ASCAT SM does not provide additional beneficial information beyond SMAP Tb at these sites, its inclusion does not degrade the forecast either, ensuring robustness without negative trade-offs. Even though there is no net improvement from the additional assimilation of ASCAT SM observations when SMAP Tb observations are assimilated, the multi-sensor assimilation system will benefit from the assimilation of ASCAT SM observations during periods when SMAP Tb observations are not available, including prior to 31 March 2015 or

during SMAP outages thereafter. During such periods, the skill of the multi-sensor system can be approximated by that of the single-sensor system that assimilates only ASCAT SM observations.

4.2 Instrumental variable approach

Validation with in-situ soil moisture observations is important but clearly very limited in its spatial coverage. To quantify the impact of the assimilation across the global domain, we employed the IV approach (section 3.4.2) using independent satellite soil moisture observations, that is, SMAP Level 3 soil moisture retrievals to assess ASC_DA, and ASCAT soil wetness retrievals to assess SMP_DA. (Recall that we cannot assess MLT_DA for lack of independent observations.) The difference in daily anomR skill between ASC_DA and CNTL is shown in Figure 3a, and the skill difference between SMP_DA and CNTL is shown in Figure 3b. In both cases, the IV approach shows a clear improvement in anomR skill following assimilation, with the mean difference being 0.06 between ASC_DA and CNTL and 0.13 between SMP_DA and CNTL. The improvement in soil moisture estimates following SMAP Tb assimilation is nearly universally larger than that following ASCAT SM assimilation, although the unavoidable use of different independent data sets complicates the comparison. The global patterns of the skill improvements over CNTL are similar for the two single-sensor assimilation experiments, with the largest improvements found across much of sub-Saharan Africa, South America and northeastern China. SMP_DA further shows strong improvement across central North America. There are some small areas of degradation with respect to CNTL that typically overlap between the two assimilation experiments, although the degradation is more extensive for ASC_DA, especially in semi-arid and arid regions. ASC_DA also shows some performance degradation in isolated pockets across the high latitudes.

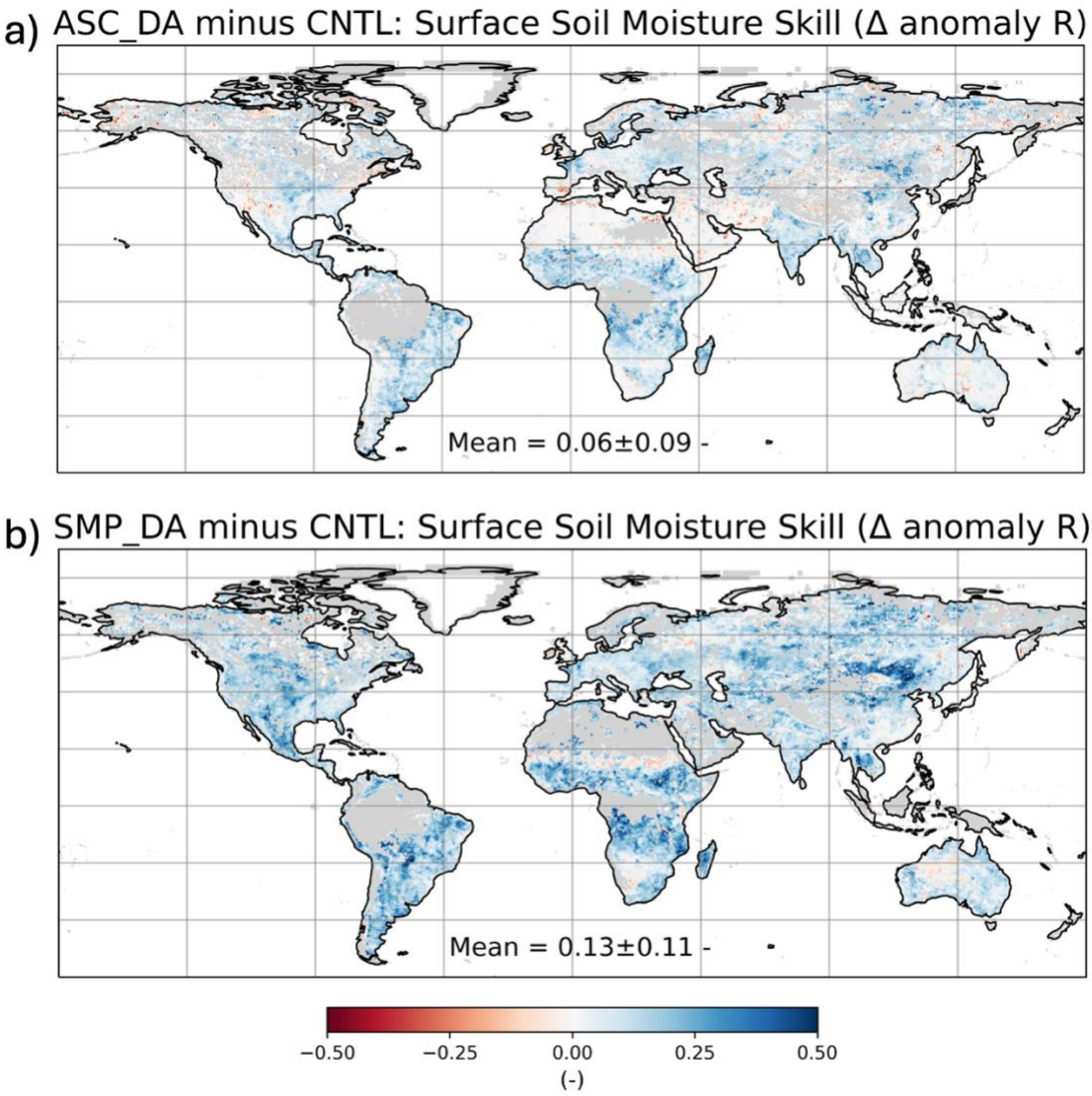

Figure 3. *Difference in surface soil moisture anomaly R (anomR) skill between (a) ASC_DA and CNTL and (b) SMP_DA and CNTL. Skill difference estimated using the IV approach (section 3.4.2) with (a) SMAP Level 3 and (b) ASCAT soil wetness as the instrumental variable for April 2015 – March 2021. Note that the instrumental variable is independent of the assimilated observations. Blue colors indicate that the assimilation improved the skill over the model-only CNTL experiment. Grey shading indicates insufficient observations available for assessment.*

4.3 Data assimilation diagnostics

4.3.1 Number of assimilated observations

Understanding the frequency of the assimilated ASCAT SM and SMAP Tb observations is key to evaluating their relative impact in a multi-sensor data assimilation system because the impact depends on the information content of individual observations as well as the

number of observations. Since the immediate impact of the land surface analysis is limited to the compact support radius of 1.25° (section 3.1), and since there is no horizontal propagation of information in the land-only assimilation system examined here, the assimilation of ASCAT SM and SMAP Tb observations cannot improve the modeled soil moisture where observations are not assimilated. Furthermore, regional variations in observation frequency could explain features in the OmF residuals or analysis increments and guide the treatment of observations.

Figure 4 shows the average number of ASCAT SM (Figure 4a) and SMAP Tb (Figure 4b) observations assimilated per day for each 36 km model grid cell over the 6 years from April 2015 to March 2021 in the MLT_DA experiment. For ASCAT, all observations of acceptable quality (section 2.2) from METOP-A, -B and -C and both ascending and descending orbits count towards the average. For SMAP, H- and V-polarization Tb observations of acceptable quality (section 2.3) from ascending and descending orbits count towards the average.

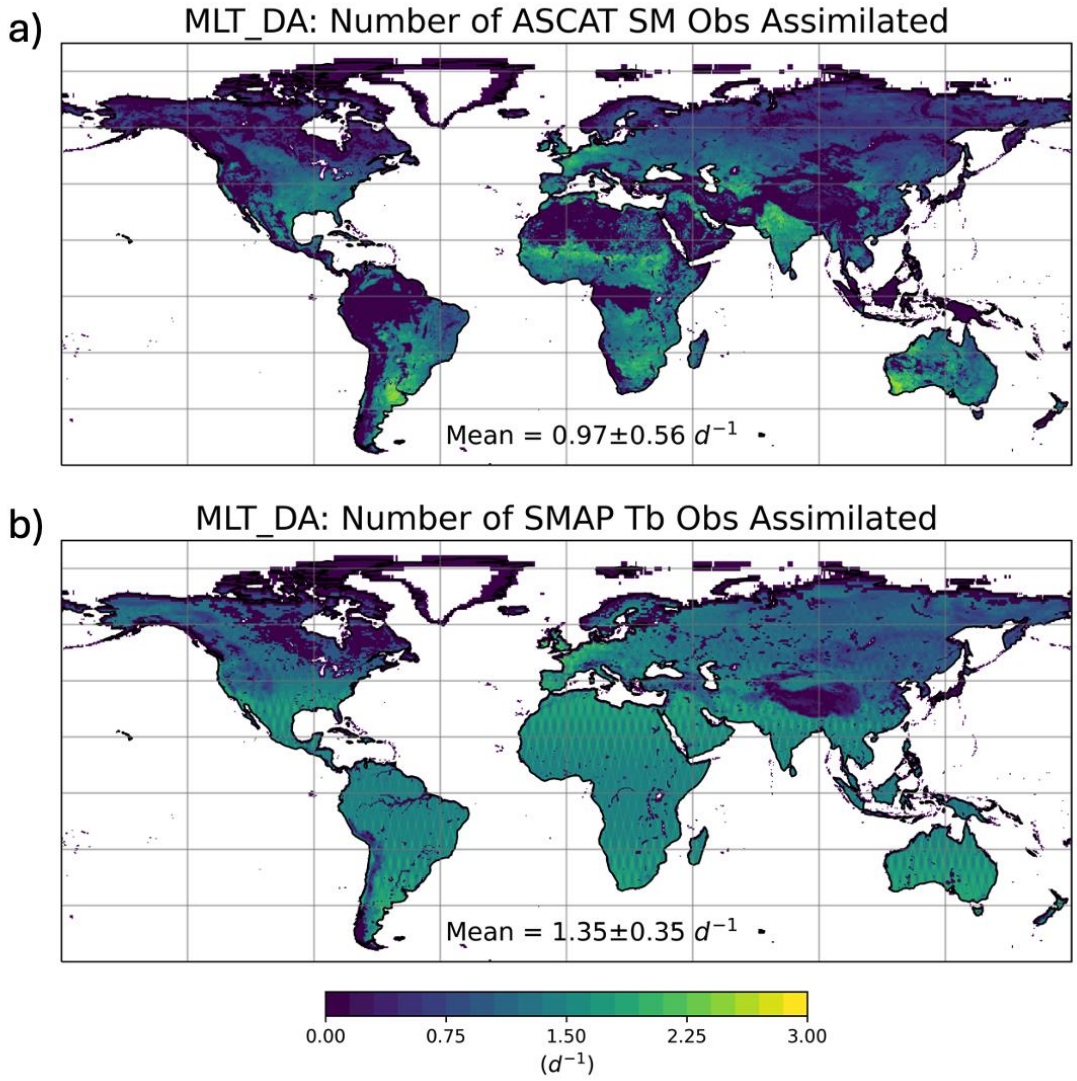

Figure 4. *Average number of (a) ASCAT SM and (b) SMAP Tb observations assimilated per day in the MLT_DA experiment during the 6-year experiment period. Averages based on (a) ASCAT observations of acceptable quality from METOP-A, -B and -C and from ascending and descending orbits and (b) SMAP H- and V-polarization observations of acceptable quality from ascending and descending orbits. Numbers in the bottom of each map indicate the spatial mean ± standard deviation.*

The global average number of observations (per 36 km grid cell) is 0.97 for ASCAT SM and 1.35 for SMAP Tb, and the maximum number (per 36 km grid cell) is 2.67 for ASCAT SM and 2.38 for SMAP Tb. The average number of assimilated SMAP Tb observations is higher than that for ASCAT SM, even though at least two, and up to three, ASCAT sensors were in orbit at any given time during the experiment period. Since the revisit time of a single ASCAT sensor is similar to that of SMAP, it is expected that the assimilation of multiple ASCAT sensors would, on average, provide more frequent SM observations than the single

SMAP sensor. However, the separate counting of the H- and V-polarization Tb observations effectively doubles the SMAP observations count. Another factor contributing to the discrepancy is the stricter QC of the ASCAT observations. As might be expected given the higher number of ASCAT sensors, the maximum number of observations in a single 36-km grid cell is higher for ASCAT SM than for SMAP Tb, as can be seen in southeastern South America and southwestern Australia (Figure 4a). QC and masking applied to ASCAT SM observations (section 2.2) means that no ASCAT SM observations are assimilated at all in the Sahara Desert and the tropical rainforests (Figure 4a). In the latter, SMAP Tb observations are routinely assimilated (Figure 4b), but owing to the typically dense vegetation, the corresponding soil moisture increments are small (section 4.3.3). For both sensors, very few or no observations are assimilated over mountainous regions (including the Rockies, Andes, and Himalayas), or near lakes or large rivers such as the Amazon. Similarly, fewer observations tend to be assimilated at high latitudes as there is only a short summer season when soils are unfrozen (and the observations pass QC), although this is partially offset by the more frequent overpasses owing to the satellites' polar orbits. For SMAP Tb, the 8-day exact repeat orbital overpasses result in a geometric pattern that is clearly visible across the lower latitudes. For ASCAT SM, the stricter QC all but erases any orbital patterns in the count of the assimilated observations.

Of the grid cells that have SMAP Tb or ASCAT SM observations at any time over the 6-year experiment period, 64% have observations from both sensors. (Note that this is different from the more likely occurrence of observations from both sensors falling within the localization distance of the spatially distributed filter and thus impacting a single grid cell's analysis increment.) However, it happens very rarely that the ASCAT and SMAP overpass times are close enough to result in the simultaneous assimilation of ASCAT SM and SMAP Tb observations during a given 3-hour analysis window at a given 36-km grid cell; this happens on average only 13.4 times per grid cell per year (or 20.7 times per grid cell per year when excluding the 36% of grid cells which never have observations from one of the two sensor types). In the high latitudes, simultaneous assimilation of ASCAT SM and SMAP Tb happens up to 101 times per grid cell per year (Figure S1a in the Supplemental Material). On average, simultaneous ASCAT SM and SMAP Tb assimilation occurs for just 1.6% of the total number of assimilated observations, although in the high latitudes the fraction can be as high as 14.8% of the total number of assimilated observations (Figure S1b in the Supplemental Material).

In summary, our results indicate that, despite some differences in QC and masking, the number and spatial distribution of assimilated ASCAT SM and SMAP Tb observations are remarkably similar. While this limits the potential of the ASCAT SM and SMAP Tb observations to complement each other, their comparable availability simplifies the assessment of their relative impacts in data assimilation. Unfortunately, both datasets exhibit reduced coverage in mountainous regions and, to a lesser extent, the high latitudes. This further supports ASCAT's role as a potential fallback option in operational weather forecasting or reanalysis applications during periods when SMAP is not available.

4.3.2 OBSERVATION-MINUS-FORECAST RESIDUALS

We first checked the mean of the OmF residuals to assess our bias correction (section 3.2). We find that the global mean (±standard deviation) of the ASCAT SM OmF residuals over the 6-year experimental period is -0.0004 (±0.0069) $m^3\ m^{-3}$ for CNTL, and the equivalent value for SMAP Tb OmF residuals is -0.03 (±0.58) K. Figure S2 in the Supplemental Material shows the global distribution of time series mean values for ASCAT SM and SMAP Tb OmF residuals for CNTL, indicating good performance nearly everywhere, except for small pockets across the high latitudes where the mean of the ASCAT SM OmF residuals can be ±0.05 $m^3\ m^{-3}$. This result implies our spatially distributed bias correction (section 3.2) adequately removes the seasonally-varying bias between the assimilated observations and the corresponding model forecasts. That is, in the long-term average the assimilation does not add or subtract water and thus does not adversely impact the global water balance.

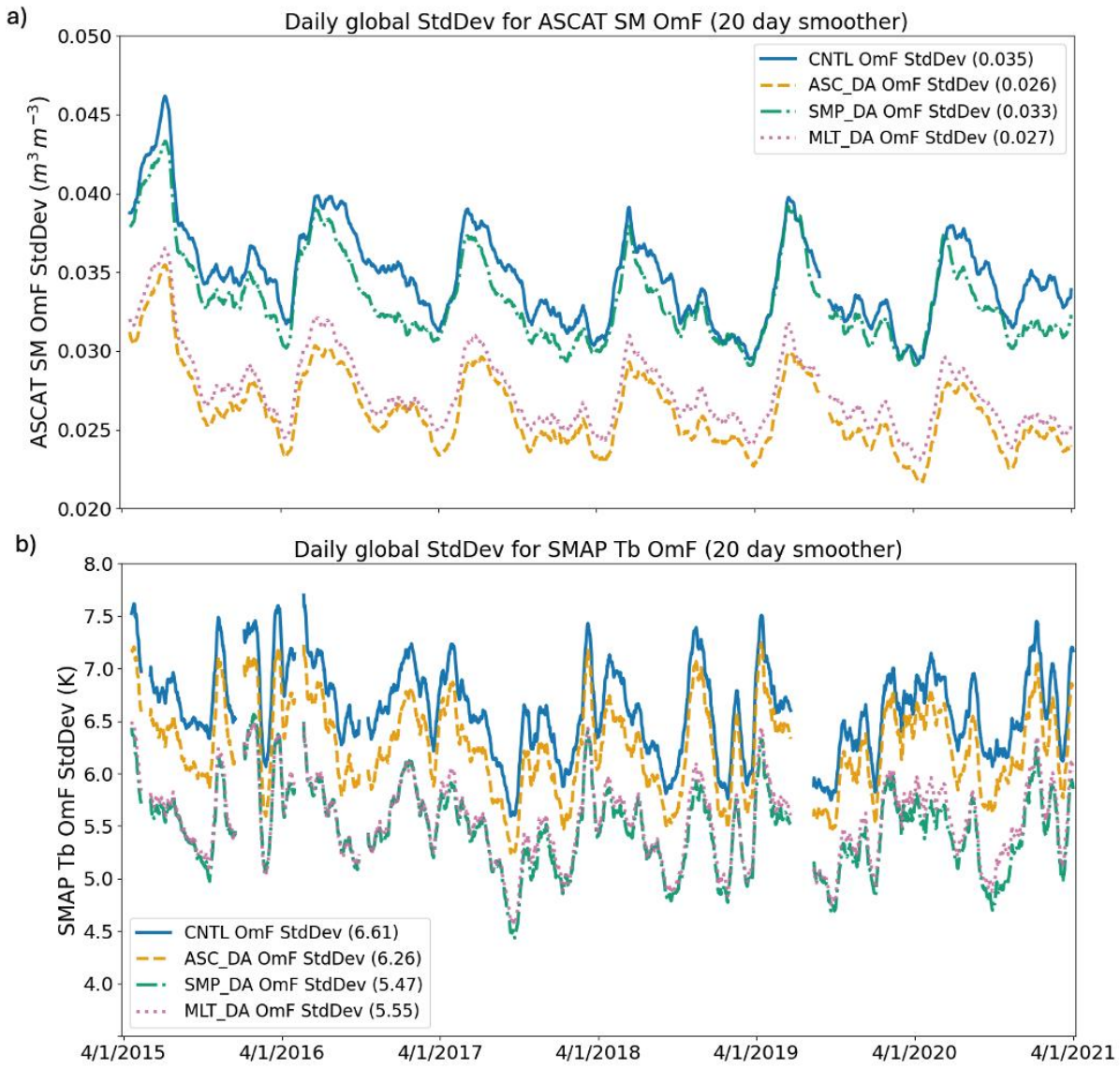

Figure 5. *Global standard deviation (StdDev) of OmF residuals for (a) ASCAT SM and (b) SMAP Tb observations from (blue solid) CNTL, (orange dashed) ASC_DA, (green dash-dot) SMP_DA, and (red dotted) MLT_DA. Standard deviation is computed from all OmF residuals within a day and then smoothed over a 20-day moving window. OmF residuals are always calculated for both observation types, including when the observations are "passive" and do not contribute to the calculation of analysis increments. The magnitude of the reduction in OmF StdDev relative to CNTL serves as an indicator of the effectiveness of the assimilation experiment. Numbers in legend indicate the time-average of the OmF global standard deviation.*

For each of the four experiments and across the 6-year experiment period, Figure 5 shows the global standard deviation of the OmF residuals for ASCAT SM and SMAP Tb. The standard deviation is computed from global OmF residuals binned into daily time periods

765 (i.e., over eight 3-hour assimilation windows) and then smoothed using a 20-day moving
766 window. For any given date, a larger OmF standard deviation in a particular experiment
767 indicates a greater mismatch between the observations and the corresponding model
768 forecasts, and thus lower skill.

769 For both observation types, the standard deviation is largest for CNTL, which can be used
770 as a benchmark (Figure 5). The ASCAT SM OmF standard deviation has a clear annual cycle
771 in all experiments (Figure 5a), with values increasing rapidly in April and peaking in the
772 Northern Hemisphere summer, most likely owing to the changing spatial support; the number
773 of assimilated observations increases in the northern latitudes as the seasonal snowpack melts
774 and soils thaw, which coincides with a relatively large variability in the observations and/or
775 forecasts. Interestingly, the OmF residuals for SMAP Tb observations do not exhibit such a
776 distinct seasonal cycle (Figure 5b), despite a similar increase in the number of observations
777 passing QC in the Northern Hemisphere during the summer months (not shown).

778 The largest reduction in the ASCAT SM OmF standard deviation occurs for ASC_DA,
779 with a relatively constant reduction of approximately 0.009 m^3 m^{-3} (Figure 5a). The reduction
780 is slightly smaller when ASCAT SM and SMAP Tb are jointly assimilated in MLT_DA.
781 There is also a small but persistent reduction in ASCAT SM OmF residuals in SMP_DA,
782 when only the SMAP Tb observations are assimilated. In this case, the ASCAT SM data are
783 passive observations and do not impact the analysis increments. This result indicates that
784 assimilating only SMAP Tb results in soil moisture forecasts that are, in the global average,
785 closer to the (passive) ASCAT observations. The relatively modest reduction of 0.002 m^3 m^{-3},
786 however, suggests that the SMAP Tb and ASCAT SM observations do not contain the same
787 information about soil moisture; if this was the case, the results for ASC_DA and SMP_DA
788 would be more similar. This indicates that while the two observation types share some
789 common sensitivity to soil moisture variability, differences in their retrieval physics and error
790 characteristics result in distinct impacts on the assimilation system.

791 The story is similar when considering the SMAP Tb OmF residuals (Figure 5b). As
792 expected, the greatest reduction in the SMAP Tb OmF standard deviation is found when
793 SMAP Tb observations are assimilated; the SMAP Tb OmF standard deviation for both
794 SMP_DA and MLT_DA is reduced by ≈1.1 K from that of CNTL in the global average
795 throughout the 6-year experiment period. In contrast, the assimilation of only ASCAT SM

observations (ASC_DA) reduces the misfit between the (passive) SMAP Tb observations and the model forecasts by just 0.3 K.

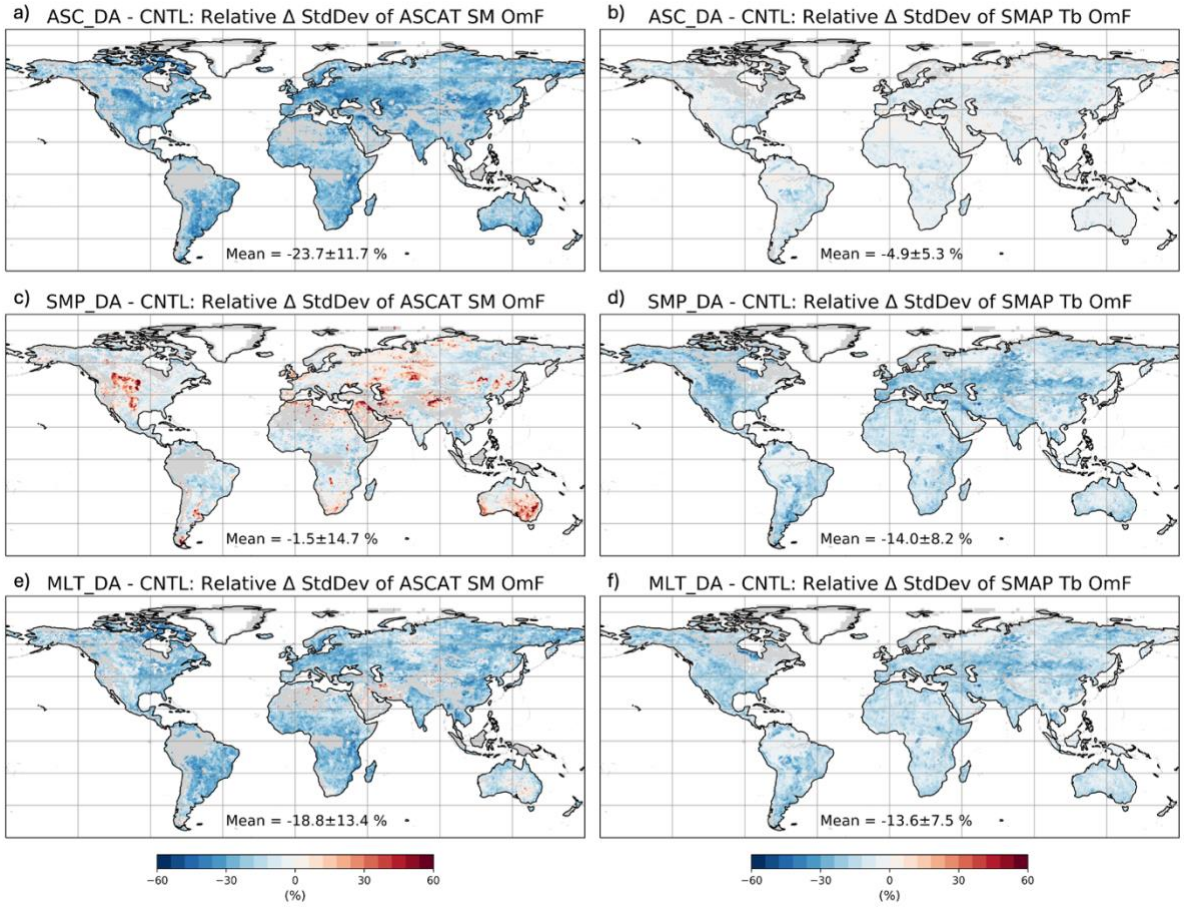

Figure 6. *Relative difference (percent) in the time series standard deviation of (a,c,e) ASCAT SM OmF residuals and (b,d,f) SMAP Tb OmF residuals between (a,b) ASC_DA and CNTL, (c,d) SMP_DA and CNTL, and (e,f) MLT_DA and CNTL. Blue shading means that the assimilation improves the model background forecasts. Relative difference is calculated with respect to the CNTL value. Metric computed for 1 April 2015 to 31 March 2021. Numbers in the bottom of each map indicate the spatial mean ± standard deviation. Grey shading indicates insufficient number of observations to calculate statistics.*

Next, Figure 6 shows the global distribution of the relative change in the time series standard deviation of the OmF residuals for the assimilation experiments with respect to that of CNTL. The relative change is the difference in the OmF standard deviation between the assimilation experiment and CNTL, normalized by the OmF standard deviation of CNTL. This metric allows for a more direct comparison of the impact of the assimilation of ASCAT SM and SMAP Tb observations, which do not share the same units. Negative values (blue

colors in Figure 6) indicate that the assimilation experiment has smaller typical OmF differences and thus has improved model background forecasts compared to those of CNTL.

For the ASCAT SM OmF standard deviation, the largest relative differences occur for ASC_DA, with a global average improvement of -23.7% (Figure 6a). There is substantial improvement in the model background forecasts nearly everywhere, including in central North America, Argentina, much of Europe, east Africa, northeastern China and eastern Australia, highlighting the global impact. A few individual grid cells, usually adjacent to masked areas and nearly invisible in Figure 6a, show some degradation, which is probably caused by minor shortcomings in the QC of the ASCAT SM observations. The reduction in the ASCAT SM OmF standard deviation shows a similar overall pattern for MLT_DA (Figure 6e), albeit with a somewhat lesser magnitude and with a few regions that exhibit a slight increase in the OmF magnitude (global average improvement of -18.8%).

As expected, the assimilation of SMAP Tb observations improved the SMAP Tb OmF standard deviation, with a global average of -14.0% for SMP_DA (Figure 6d) and -13.6% for MLT_DA (Figure 6f). Both experiments show very similar spatial patterns of improvement. Across the globe, locations where SMAP observations are assimilated generally show some improvement, with the largest differences in central North America, along the southern shore of Hudson Bay, Argentina, western Europe, Kazakhstan, central Russia, and along the river plains of northern India.

There is a modest but nearly universal reduction (-4.9% on average) in the magnitude of the SMAP Tb OmF residuals when only ASCAT SM is assimilated in ASC_DA (Figure 6b). That is, assimilating ASCAT SM adjusts model forecasts of soil moisture such that the simulated Tb is closer to the (passive) SMAP Tb observations. The impact of assimilating only SMAP Tb on forecasts of ASCAT SM is slightly beneficial overall, with a global average of -1.5% (Figure 6c). But the slight average improvement is the result of a balance between modest improvements across large areas and more marked degradation in smaller pockets across central North America, southeastern Australia, northern Africa, and the Middle East. Interestingly, some of the areas with the most marked degradation of the ASCAT SM OmF standard deviation in SMP_DA match those with the biggest improvements from the assimilation of only ASCAT SM in ASC_DA. That is, discrepancies between ASCAT SM and SMAP Tb observations lead to contrasting updates in ASC_DA and SMP_DA, respectively, thereby degrading model forecasts in SMP_DA relative to the

(passive) ASCAT SM observations. In the MLT_DA experiment, there is a slight degradation in the ASCAT SM OmF standard deviation in some of the same areas, especially across the hot deserts of the Middle East and southeastern Australia (Figure 6e). Nevertheless, as mentioned above, the joint assimilation of both observation types in MLT_DA still results in significant reductions in the magnitude of the ASCAT SM OmF residuals (Figure 6e).

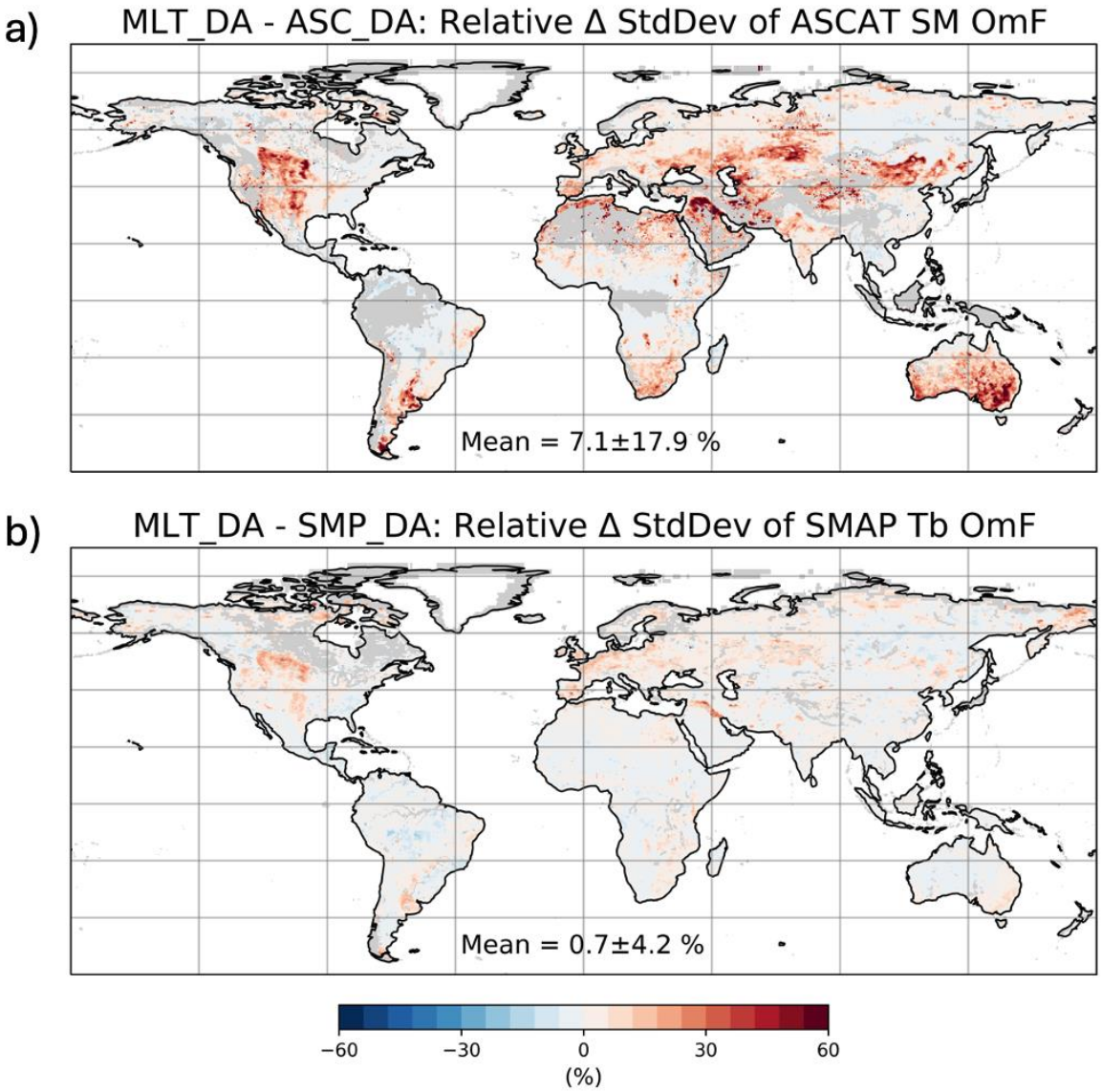

***Figure** 7. Relative difference (percent) in the time series standard deviation (a) of ASCAT SM OmF residuals between MLT_DA and ASC_DA and (b) of SMAP Tb OmF residuals between MLT_DA and SMP_DA. Relative difference is calculated with respect to (a) the ASC_DA value and (b) the SMP_DA value. Red shading means that the assimilation results in degraded model background forecasts. Metric computed for 1 April 2015 to 31 March 2021. Numbers in the bottom of each map indicate the spatial mean ± standard deviation. Grey shading indicates insufficient number of observations to calculate statistics.*

Figure 7 again shows the relative change (in percent) in the time series standard deviation of the OmF residuals, but instead of comparing with CNTL as in Figure 6, the difference is now between MLT_DA and the single-sensor assimilation experiments. The figure highlights that MLT_DA has larger OmF residuals than do the corresponding single-sensor experiments, in agreement with the results of Figures 5 and 6. In the global average, the ASCAT SM OmF standard deviation increases by 7.1% in MLT_DA relative to ASC_DA (Figure 7a), while the SMAP Tb OmF standard deviation increases by only 0.7% in MLT_DA relative to SMP_DA (Figure 7b). Since MLT_DA assimilates approximately double the number of observations than does ASC_DA, a small increase in the variability of the OmF residuals can be expected. But increases in excess of 30% are seen for the magnitude of the ASCAT SM OmF residuals in central North America, the Middle East, and southeastern Australia (Figure 7a). In these locations, the soil moisture information from the ASCAT SM and SMAP Tb observations is presumably in poor agreement, and competing updates from each observation type results in larger misfits between the ASCAT SM observations and the corresponding model background forecasts. The slightly larger OmF residuals in MLT_DA compared to ASC_DA and SMP_DA suggest the need for error parameterization strategies that account for regional differences in observation reliability and consistency to ensure that jointly assimilating multiple data sources does not inadvertently degrade the forecast skill.

In contrast, additionally assimilating ASCAT SM in MLT_DA has a more neutral impact on the magnitude of the SMAP Tb OmF residuals relative to the SMP_DA single-sensor experiment (Figure 7b). This is consistent with what is seen for the passive observations in the single-sensor assimilation experiments; when SMAP Tb observations are assimilated in SMP_DA, the magnitude of the ASCAT SM OmF residuals increased considerably in many areas, even though the overall impact is neutral (Figure 6c). Conversely, assimilating ASCAT SM in ASC_DA caused a modest decrease in the magnitude of the SMAP Tb OmF residuals (Figure 6b). The relatively smaller observation error of SMAP Tb compared to that of ASCAT SM (section 3.1) leads to contrasting magnitudes in the associated increments (section 4.3.3), which may partially explain the relatively larger impact on ASCAT SM OmF residuals in SMP_DA compared to the more modest impact on SMAP Tb OmF residuals in ASC_DA.

4.3.3 Analysis increments

The EnKF uses the OmF residuals to calculate analysis increments for the CLSM prognostic variables srfexc and rzexc (and catdef for peatland grid cells; section 3.1) that are then applied to the corresponding model prognostic variables. Increments in (volumetric) surface and root-zone soil moisture can be diagnosed by differencing the corresponding analysis and forecast soil moisture values. Given the spatially distributed approach to filtering, an analysis increment computed for a given grid cell is typically influenced by several observations within the localization radius. Consequently, analysis increments are also computed for grid cells that are not directly observed; this is accomplished by combining the non-local observational information with information from the horizontal error correlations. Therefore, the global pattern of the number of analysis increments should resemble that of the number of assimilated observations after some spatial interpolation and extrapolation.

The global distribution of the number of increments per day in each of the assimilation experiments is shown in Figure 8, indicating how often the simulated soil moisture is updated at a given location in response to ASCAT or SMAP observations. For the assimilation of ASCAT SM observations, Figure 8a shows how increments extend well into areas where ASCAT SM observations are masked for QC reasons (Figure 4a), for example around tropical rainforest areas in Amazonia and the Congo, the mountainous regions of Asia and western North America, and the Sahara Desert. In the global average, the number of increments per day for ASC_DA is 1.21, approximately 25% more than the average number of assimilated ASCAT SM observations (mean = 0.97 d^{-1}).

The number of analysis increments for SMP_DA (mean = 0.69 d^{-1}; Figure 8b) seems surprising low relative to the number of assimilated SMAP Tb observations (mean = 1.35 d^{-1}; Figure 4b), but there is a simple explanation. H- and V-polarization Tb observations are counted as separate observations in Figure 4, but for a given location and overpass time, they are almost always available simultaneously and assimilating a V-polarization Tb observation at the same time and location where there is already an H-polarization Tb observation does not result in an additional analysis increment. Counting each pair of H- and V-polarization Tbs as a single observation, the global average number of assimilated SMAP Tb observations drops to 0.67 per day. Therefore, the number of analysis increments in SMP_DA corresponds very closely with the number of assimilated Tb observations, and the relative difference

between the number of increments and assimilated observations is much smaller than for the assimilation of ASCAT SM.

Finally, the total number of assimilated observations for MLT_DA is given by the sum of the assimilated ASCAT SM (Figure 4a) and the assimilated SMAP Tb (Figure 4b). (These numbers are nearly identical for the respective single-sensor assimilation experiments because the model-based QC of the observations differs only slightly between the single- and multi-sensor assimilation experiment; not shown.) Counting again only the number of pairs of H- and V-polarization Tb observations yields a global average of 1.64 assimilated observations per day in MLT_DA, compared to a global average of 1.78 increments per day (Figure 8c). As discussed above, ASCAT SM and SMAP Tb observations are assimilated simultaneously for only 1.6% of the total number of assimilated observations (section 4.3.1). Yet the number of increments per day in MLT_DA (mean=1.78 d^{-1}) is ~10% less than the sum of the number of increments per day from ASC_DA and SMP_DA. This can be explained because the spatial interpolation and extrapolation associated with the computation of the analysis increments in MLT_DA is less efficient than in the single-sensor assimilation experiments, owing to the larger number of assimilated observations in MLT_DA.

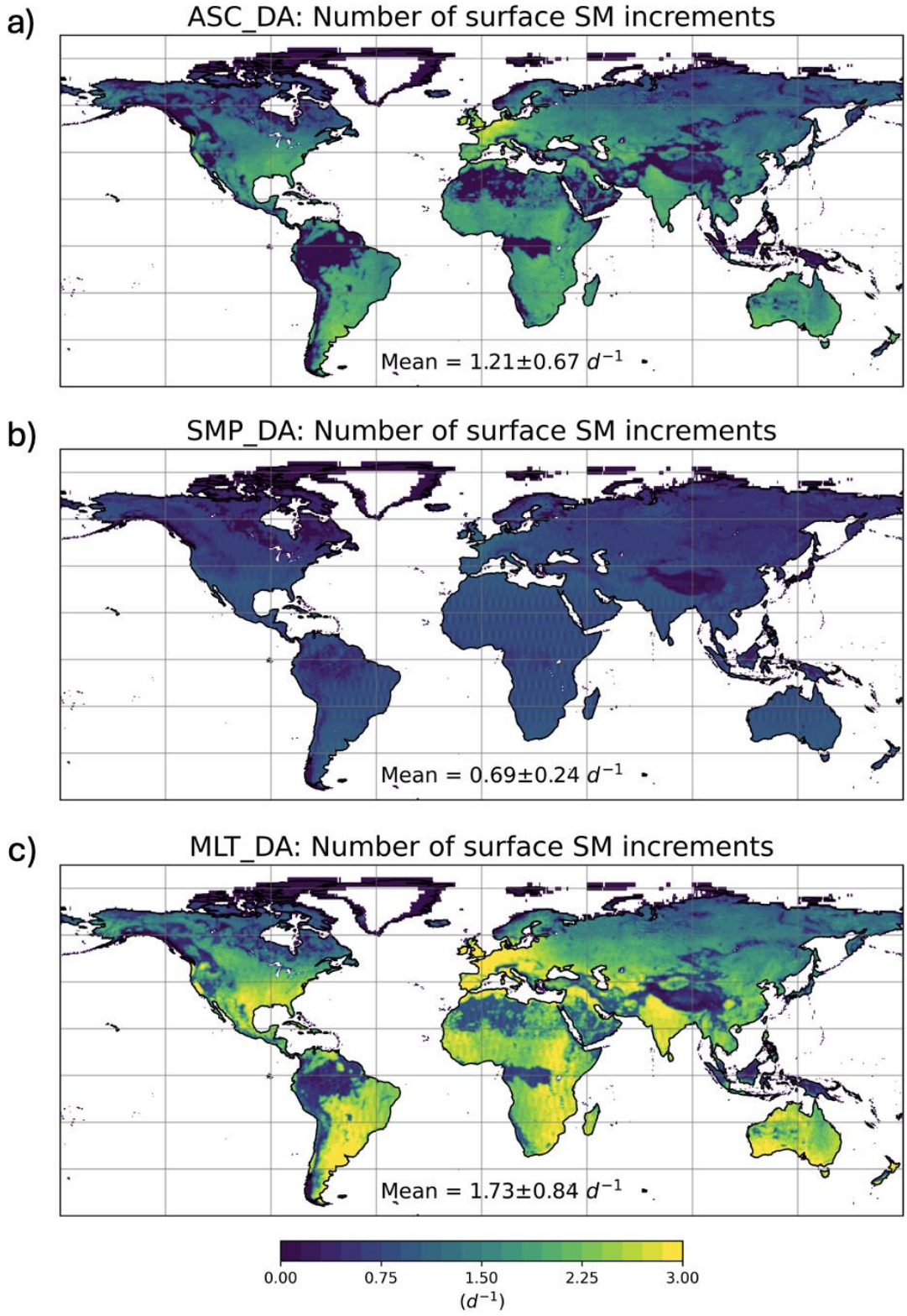

939

940 ***Figure 8***. *Average number of surface soil moisture analysis increments per day during*
941 *the 6-year experiment period for (a) ASC_DA, (b) SMP_DA and (c) MLT_DA. Numbers in*
942 *the bottom of each map indicate the spatial mean ± standard deviation.*

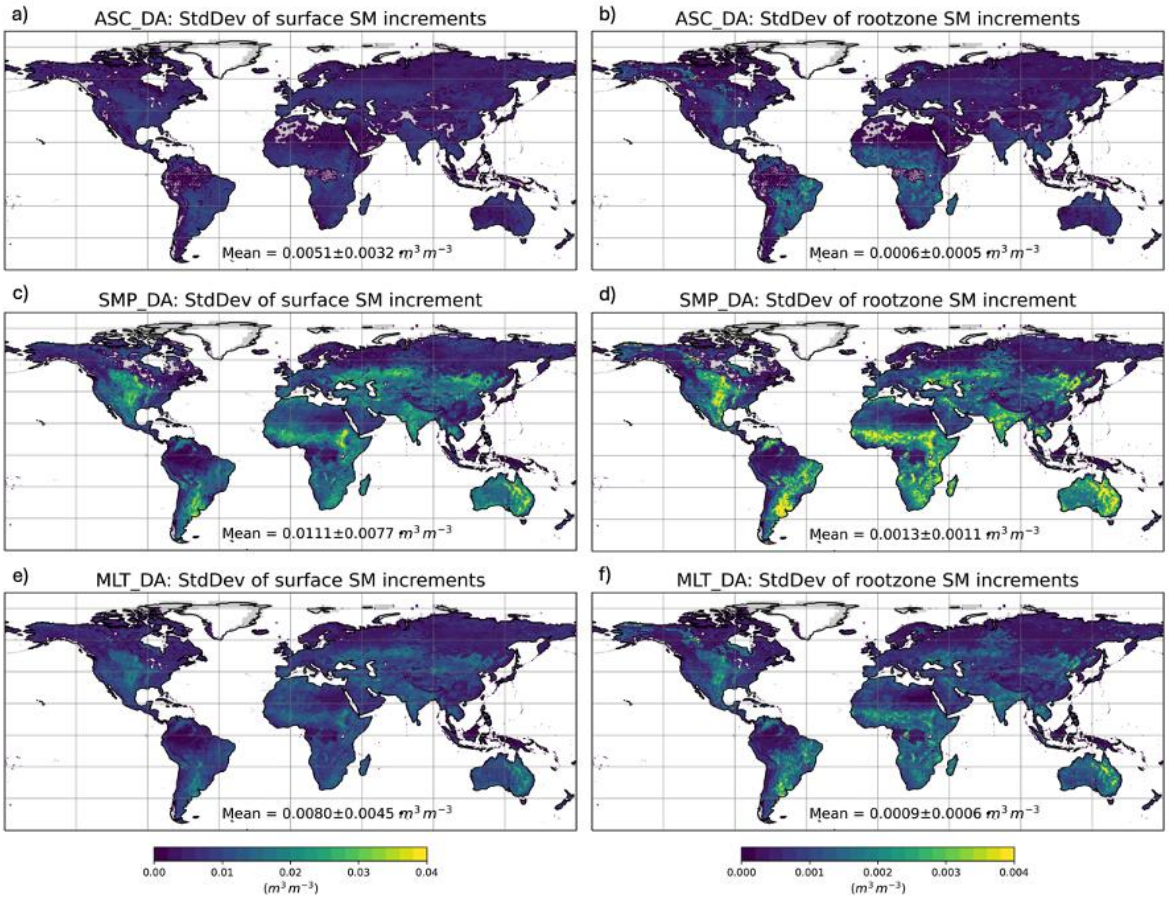

Figure 9. *Time series standard deviation of analysis increments for (a,c,e) surface soil moisture and (b,d,f) root-zone soil moisture from (a,b) ASC_DA, (c,d) SMP_DA, and (e,f) MLT_DA. Metric computed for 1 April 2015 to 31 March 2021. Numbers in the bottom of each map indicate the spatial mean ± standard deviation. Grey shading indicates insufficient number of observations to calculate statistics.*

Figure 9 shows the time series standard deviation (or typical magnitude) of the surface and root-zone soil moisture analysis increments from each assimilation experiment. For all experiments, the analysis increments are largest in central North America, Argentina, the Sahel, mid-latitude Eurasia, India, and much of Australia. The largest increments are generally found where the magnitude of the OmF residuals is reduced the most by the assimilation (that is, relative to CNTL; Figure 6). However, none of the experiments have large increments in the high latitudes, despite the reduction in the magnitude of the OmF residuals there. The average magnitude of the increments differs greatly across the experiments. For the surface soil moisture increments, the global average magnitude is 0.0111 m^3 m^{-3} for SMP_DA, which is double the 0.0051 m^3 m^{-3} value for ASC_DA. Similarly, for root-zone soil moisture increments the global average is 0.0013 m^3 m^{-3} for

SMP_DA and 0.0006 m^3 m^{-3} for ASC_DA. That is, while there are only about half as many analysis increments in SMP_DA than in ASC_DA (Figure 8a, b), the magnitude of the increments in SMP_DA is typically double that in ASC_DA. As expected, the typical magnitude of the analysis increments in MLT_DA is 0.0080 m^3 m^{-3} for surface soil moisture and 0.0009 m^3 m^{-3} for root-zone soil moisture, which falls between those of ASC_DA and SMP_DA. This difference in the magnitude of the increments between the observation types is most likely explained by the relatively smaller observation error ascribed to the SMAP Tb observations, and thus the larger adjustment of modeled soil moisture towards the observations. Surface soil moisture increments are roughly an order of magnitude larger than root-zone soil moisture increments because the srfexc prognostic variable has much stronger error correlations with the assimilated surface soil moisture and brightness temperature than does the rzexc prognostic variable.

5. Summary and Conclusion

This paper describes how we added the capability to assimilate ASCAT SM observations to GEOS LDAS, a well validated data assimilation system that assimilates SMAP Tb observations operationally to generate the L4_SM soil moisture assimilation product. We document our approach to ASCAT SM observation QC and bias correction, and we briefly describe the system setup and our validation methodologies. The latter include comparisons to in-situ soil moisture measurements and independent satellite observations as well as the examination of a suite of data assimilation diagnostics. We conducted a series of simulation and assimilation experiments to investigate the impact of assimilating ASCAT SM and SMAP Tb observations on global soil moisture estimates. Relative to a model-only CLSM simulation without satellite data assimilation, we assess the effect of assimilating only ASCAT SM observations, assimilating only SMAP Tb observations, and jointly assimilating both observation types.

Our results show that assimilating ASCAT SM observations universally improves soil moisture estimates over those of the model-only CLSM simulation. In-situ measurements confirmed this to be true for both surface and root-zone soil moisture (Figure 2), and comparison with SMAP Level 3 soil moisture observations using the IV approach indicated a widespread global distribution for these improvements (Figure 3). We further found that

assimilating only SMAP Tb observations yielded noticeably better improvements in soil moisture estimates (using ASCAT SM observations in the IV approach). Jointly assimilating both observation types gave results very similar to assimilating SMAP Tb observations alone. These results support our expectation that the SMAP Tb observations provide more accurate information about surface soil moisture conditions, which has been documented in several previous studies. Despite the known limitations of the ASCAT SM observations, they nevertheless provide valuable information that enables our data assimilation system to improve soil moisture estimates.

A close examination of a suite of data assimilation diagnostics allowed us to investigate how the system responds to the assimilation of the different observation types. The average number of observations assimilated was similar for ASCAT SM and SMAP Tb (Figure 4), even though up to three ASCAT sensors were in orbit during our experiment period compared to just one SMAP satellite. This is readily explained by the necessarily stricter QC applied to the ASCAT SM observations and the separate counting of H- and V-polarization SMAP Tb observations. Neither observation type offered good coverage over mountainous regions. Although both sensors are in polar orbits, the number of assimilated observations in the high latitudes was limited, owing to the short summer season of unfrozen soils there. The number of assimilation windows that simultaneously contain both observation types at a given location is greatest in the high latitudes, owing to the sensors' polar orbits. Such simultaneous assimilation of ASCAT SM and SMAP Tb observations happens relatively rarely outside of the high latitudes.

Over the 6-year experiment period, the mean of the ASCAT SM and SMAP Tb OmF residuals was found to be close to zero, indicating that our bias correction approach (section 3.2) worked well and that the assimilation does not adversely impact the model's water balance over the long term. We used the magnitude of the times series standard deviation of the OmF residuals as an indicator of the typical magnitude of the OmF residuals and quantified its reduction as a measure of the effectiveness of the assimilation. As expected, we found the largest reductions in OmF residuals specific to the observation type being assimilated. More interestingly, we found that assimilating ASCAT SM observations alone reduced the magnitude of SMAP Tb OmF residuals globally (Figures 5 and 6), implying some agreement between the ASCAT SM and SMAP Tb observations. This result was corroborated with the IV validation. The assimilation of only SMAP Tb observations had a

more neutral impact on the verification of the soil moisture estimates against the passive (i.e., not assimilated) ASCAT Tb observations.

We found that the assimilation of both types of observations in the multi-sensor assimilation experiment had an overall similar impact on the OmF residuals as that of the corresponding single-sensor assimilation experiment, albeit with somewhat larger OmF residuals in the multi-sensor assimilation experiment than in the corresponding single-sensor experiments (Figure 7). This suggests that the information from ASCAT SM and SMAP Tb observations does not always agree, and that competing analysis increments from the two observation types can result in larger misfits between the observations and the forecasts.

Moreover, we found that both observation types tend to result in the largest adjustments of the modeled soil moisture in similar places (where OmF residuals are also the largest). The increments resulting from assimilating SMAP Tb observations tend to be larger but occur less frequently than those from assimilating ASCAT SM observations, owing to the greater number of assimilated ASCAT SM observations (when counting H- and V-polarization observations in pairs) and their relatively larger assigned observation error standard deviation (Figures 4, 8 and 9).

In agreement with expectation, all validation approaches suggest that assimilating ASCAT SM observations improves soil moisture analysis estimates, though to a lesser extent than does SMAP Tb assimilation. Nevertheless, adding ASCAT SM to GEOS LDAS is clearly beneficial, with broader implications for future operational forecasting systems and global reanalysis datasets.

Our results indicate that assimilating soil moisture observations from multiple sensors enhances the robustness of an LDAS, ensuring that useful observational constraints remain even when one dataset is unavailable or has higher uncertainties. Here, we demonstrate that assimilating ASCAT SM alone is still superior to a model-only CLSM simulation, allowing the system to "fall back" on available observations. Furthermore, ASCAT SM records extend back to May 2007, providing nearly eight additional years of historical soil moisture information for reanalysis before the advent of SMAP Tb observations in 2015. Incorporating multiple soil moisture observations into an LDAS enables long-term consistency in soil moisture estimates for both the surface and root zone, a critical factor for climate monitoring and hydrological applications that depend on reliable estimates of long-term soil moisture variability.

Our analysis of the OmF residuals highlights that integrating multiple soil moisture datasets requires careful handling of systematic differences in the observations and the model estimates. Differences in error characteristics, retrieval algorithms, and spatiotemporal sampling may introduce competing updates. This was seen in the multi-sensor experiment, where the typical magnitude of the ASCAT SM OmF residuals increased relative to that of the single-sensor experiments. While this effect did not significantly degrade the overall analysis, it underscores the potential for conflicting information from different sensors, leading to competing analysis increments.

To mitigate such effects, next steps would be to develop techniques that incorporate region-specific observation error and/or dynamically adjust the influence of observations based on land surface conditions and seasonality. Another approach to improve uncertainty quantification may be the direct assimilation of ASCAT radar backscatter (Lievens et al. 2017). However, this requires a fast and accurate observation operator for radar backscatter, which remains challenging over heterogeneous surfaces. Future advancements in machine learning-based observation operators could help bridge this gap, enabling more effective assimilation of ASCAT backscatter and further improving soil moisture estimates (Aires et al., 2021).

Looking ahead, it will be important to incorporate ASCAT SM observations, along with additional satellite observations of soil moisture or L-band Tb (such as from SMOS), into the GEOS weakly-coupled land-atmosphere data assimilation system, which will allow us to assess the impact of the additional land surface observations on the skill of medium-range weather forecasts. The spatial and temporal patterns of multi-sensor soil moisture increments may have an impact on weather forecasts that is different from that resulting from the overall increase in the soil moisture estimation skill documented here.

There is a long and growing list of land surface observations that can potentially be used to produce land surface reanalyses for a variety of purposes (Baatz et al., 2021; De Lannoy et al., 2022; Kumar et al., 2022). The approach and results documented here provide an outline for how to extend a state-of-the-science LDAS to include additional and complementary types of observations and thoroughly evaluate their impact.

Acknowledgments.

Funding for this work was provided by the SMAP mission, the SMAP Science Team, and the NASA Modeling, Analysis, and Prediction program. Computational resources were provided by the NASA High-End Computing program through the NASA Center for Climate Simulation. For the in situ validation data we thank S. Bircher, A. Colliander, Á. González-Zamora, K. H. Jensen, E. Lopez-Baeza, J. Martínez-Fernández, T. Pellarin, M. Thibeault, J. P. Walker, and X. Wu.

Data Availability Statement.

The SMAP Level 1C brightness temperature and Level 3 soil moisture observations, ancillary inputs, and the in-situ soil moisture measurements used for validation are available from http://nsidc.org/data/smap. Output from the CNTL, ASC_DA, SMP_DA and MLT_DA experiments can be obtained from https://gmao.gsfc.nasa.gov/gmaoftp/amfox/datasets/JHM-Oct24/. GEOS forcing data are available from https://fluid.nccs.nasa.gov/weather. ASCAT soil moisture data are available from the European Organisation for the EUMETSAT Hydrology Satellite Application Facility at https://www.eumetsat.int/h-saf. The GEOS source code is released under the NASA Open-Source Agreement at http://opensource.gsfc.nasa.gov/projects/GEOS-5 and available from https://github.com/GEOS-ESM/GEOSldas/releases. GEOS LDAS release v18.0.3 was used for this study.

1107 REFERENCES

1108 Aires, F., Weston, P., Rosnay, P., & Fairbairn, D. (2021). Statistical approaches to assimilate
1109 ASCAT soil moisture information—I. Methodologies and first assessment. *Quart. J. Roy.*
1110 *Meteor. Soc.*, *147*(736), 1823–1852. https://doi.org/10.1002/qj.3997

1111 Al-Yaari, A., Wigneron, J.-P., Dorigo, W., Colliander, A., Pellarin, T., Hahn, S., Mialon, A.,
1112 Richaume, P., Fernandez-Moran, R., Fan, L., Kerr, Y. H., & De Lannoy, G. (2019).
1113 Assessment and inter-comparison of recently developed/reprocessed microwave satellite
1114 soil moisture products using ISMN ground-based measurements. *Remote Sensing of*
1115 *Environment*, *224*, 289–303. https://doi.org/10.1016/j.rse.2019.02.008

1116 Baatz, R., Franssen, H. J. H., Euskirchen, E., Sihi, D., Dietze, M., Ciavatta, S., Fennel, K.,
1117 Beck, H., De Lannoy, G., Pauwels, V. R. N., Raiho, A., Montzka, C., Williams, M.,
1118 Mishra, U., Poppe, C., Zacharias, S., Lausch, A., Samaniego, L., Van Looy, K., …
1119 Vereecken, H. (2021). Reanalysis in earth system science: Towards terrestrial ecosystem
1120 reanalysis. *Rev. Geophys.* https://doi.org/10.1029/2020rg000715

1121 Balsamo, G., Agustì-Parareda, A., Albergel, C., Arduini, G., Beljaars, A., Bidlot, J.,
1122 Bousserez, N., Boussetta, S., Brown, A., Buizza, R., Buontempo, C., Chevallier, F.,
1123 Choulga, M., Cloke, H., Cronin, M. F., Dahoui, M., De Rosnay, P., Dirmeyer, P. A.,
1124 Drusch, M., … Zeng, X. (2018). Satellite and In Situ Observations for Advancing Global
1125 Earth Surface Modelling: A Review. *Remote Sensing*, *10*(12), 2038.
1126 https://doi.org/10.3390/rs10122038

1127 Bartalis, Z., Naeimi, V., Hasenauer, S., & Wagner, W. (2008). *ASCAT Soil Moisture Product*
1128 *Handbook | EUMETSAT* (15; Report Series). Institute of Photogrammetry and Remote
1129 Sensing, Vienna University of Technology. https://www-cdn.eumetsat.int/files/2020-
1130 04/pdf_soilmoisture_prod_hb.pdf

1131 Bartalis, Z., Wagner, W., Naeimi, V., Hasenauer, S., Scipal, K., Bonekamp, H., Figa, J., &
1132 Anderson, C. (2007). Initial soil moisture retrievals from the METOP-A Advanced
1133 Scatterometer (ASCAT). *Geophys. Res. Lett.*, *34*(20).
1134 https://doi.org/10.1029/2007gl031088

1135 Beck, H. E., Pan, M., Miralles, D. G., Reichle, R. H., Dorigo, W. A., Hahn, S., Sheffield, J.,
1136 Karthikeyan, L., Balsamo, G., Parinussa, R. M., van Dijk, A. I. J. M., Du, J., Kimball, J.
1137 S., Vergopolan, N., & Wood, E. F. (2021). Evaluation of 18 satellite- and model-based

soil moisture products using in situ measurements from 826 sensors. *Hydrol. Earth Syst. Sci.*, *25*(1), 17–40. https://doi.org/10.5194/hess-25-17-2021

Bojinski, S., Verstraete, M., Peterson, T. C., Richter, C., Simmons, A., & Zemp, M. (2014). *The Concept of Essential Climate Variables in Support of Climate Research, Applications, and Policy*. https://doi.org/10.1175/BAMS-D-13-00047.1

Brodzik, M. J., Billingsley, B., Haran, T., Raup, B., & Savoie, M. H. (2012). EASE-Grid 2.0: Incremental but Significant Improvements for Earth-Gridded Data Sets. *ISPRS International Journal of Geo-Information*, *1*(1), Article 1. https://doi.org/10.3390/ijgi1010032

Carrera, M. L., Bélair, S., & Bilodeau, B. (2015). The Canadian Land Data Assimilation System (CaLDAS): Description and Synthetic Evaluation Study. *J. Hydrometeorol.*, *16*(3), 1293–1314. https://doi.org/10.1175/JHM-D-14-0089.1

Carrera, M. L., Bilodeau, B., Bélair, S., Abrahamowicz, M., Russell, A., & Wang, X. (2019). Assimilation of Passive L-band Microwave Brightness Temperatures in the Canadian Land Data Assimilation System: Impacts on Short-Range Warm Season Numerical Weather Prediction. *J. Hydrometeorol.*, *20*(6), 1053–1079. https://doi.org/10.1175/JHM-D-18-0133.1

Chan, S., Njoku, E. G., & Colliander, A. (2023). *SMAP L1C Radiometer Half-Orbit 36 km EASE-Grid Brightness Temperatures, Version 6* [Dataset]. NASA National Snow and Ice Data Center Distributed Active Archive Center. https://doi.org/10.5067/DV7IX2DQ681Y

Chen, F., Crow, W. T., Bindlish, R., Colliander, A., Burgin, M. S., Asanuma, J., & Aida, K. (2018). Global-scale evaluation of SMAP, SMOS and ASCAT soil moisture products using triple collocation. *Remote Sensing of Environment*, *214*, 1–13. https://doi.org/10.1016/j.rse.2018.05.008

Colliander, A., Jackson, T. J., Bindlish, R., Chan, S., Das, N., Kim, S. B., Cosh, M. H., Dunbar, R. S., Dang, L., Pashaian, L., Asanuma, J., Aida, K., Berg, A., Rowlandson, T., Bosch, D., Caldwell, T., Caylor, K., Goodrich, D., al Jassar, H., … Yueh, S. (2017). Validation of SMAP surface soil moisture products with core validation sites. *Remote Sensing of Environment*, *191*, 215–231. https://doi.org/10.1016/j.rse.2017.01.021

Colliander, A., Reichle, R. H., Crow, W. T., Cosh, M. H., Chen, F., Chan, S., Das, N. N., Bindlish, R., Chaubell, J., Kim, S., Liu, Q., O'Neill, P. E., Dunbar, R. S., Dang, L. B.,

Kimball, J. S., Jackson, T. J., Al-Jassar, H. K., Asanuma, J., Bhattacharya, B. K., … Yueh, S. H. (2022). Validation of Soil Moisture Data Products From the NASA SMAP Mission. *IEEE Journal of Selected Topics in Applied Earth Observations and Remote Sensing*, *15*, 364–392. IEEE Journal of Selected Topics in Applied Earth Observations and Remote Sensing. https://doi.org/10.1109/JSTARS.2021.3124743

Crow, W. T., Berg, A. A., Cosh, M. H., Loew, A., Mohanty, B. P., Panciera, R., de Rosnay, P., Ryu, D., & Walker, J. P. (2012). Upscaling sparse ground-based soil moisture observations for the validation of coarse-resolution satellite soil moisture products. *Reviews of Geophysics*, *50*(2). https://doi.org/10.1029/2011RG000372

Crow, W. T., Dong, J., & Reichle, R. H. (2022). Leveraging Pre-Storm Soil Moisture Estimates for Enhanced Land Surface Model Calibration in Ungauged Hydrologic Basins. *Water Resources Research*, *58*(8), e2021WR031565. https://doi.org/10.1029/2021WR031565

Dawdy, D., & Matalas, N. (1964). Statistical and probability analysis of hydrologic data, part III: Analysis of variance, covariance and time series. In *Handbook of Applied Hydrology: A Compendium of Water-Resources Technology* (Vol. 8, Issue 8.90). McGraw-Hill.

De Lannoy, G. J. M., Bechtold, M., Albergel, C., Brocca, L., Calvet, J.-C., Carrassi, A., Crow, W. T., de Rosnay, P., Durand, M., Forman, B., Geppert, G., Girotto, M., Hendricks Franssen, H.-J., Jonas, T., Kumar, S., Lievens, H., Lu, Y., Massari, C., Pauwels, V. R. N., … Steele-Dunne, S. (2022). Perspective on satellite-based land data assimilation to estimate water cycle components in an era of advanced data availability and model sophistication. *Frontiers in Water*, *4*. https://doi.org/10.3389/frwa.2022.981745

De Lannoy, G. J. M., De Rosnay, P., & Reichle, R. H. (2019). Soil Moisture Data Assimilation. In Q. Duan, F. Pappenberger, A. Wood, H. L. Cloke, & J. C. Schaake (Eds.), *Handbook of Hydrometeorological Ensemble Forecasting* (pp. 701–743). Springer Berlin Heidelberg. https://doi.org/10.1007/978-3-642-39925-1_32

De Lannoy, G. J. M. D., Reichle, R. H., & Pauwels, V. R. N. (2013). *Global Calibration of the GEOS-5 L-Band Microwave Radiative Transfer Model over Nonfrozen Land Using SMOS Observations*. https://doi.org/10.1175/JHM-D-12-092.1

1198 De Lannoy, G. J. M., & Reichle, R. H. (2016a). Assimilation of SMOS brightness
1199 temperatures or soil moisture retrievals into a land surface model. *Hydrol. Earth Syst.*
1200 *Sci.*, *20*(12), 4895–4911. https://doi.org/10.5194/hess-20-4895-2016

1201 De Lannoy, G. J. M., & Reichle, R. H. (2016b). Global Assimilation of Multiangle and
1202 Multipolarization SMOS Brightness Temperature Observations into the GEOS-5
1203 Catchment Land Surface Model for Soil Moisture Estimation. *J. Hydrometeorol.*, *17*(2),
1204 669–691. https://doi.org/10.1175/JHM-D-15-0037.1

1205 De Lannoy, G. J. M., Reichle, R. H., & Vrugt, J. A. (2014). Uncertainty quantification of
1206 GEOS-5 L-band radiative transfer model parameters using Bayesian inference and SMOS
1207 observations. *Remote Sensing of Environment*, *148*, 146–157.
1208 https://doi.org/10.1016/j.rse.2014.03.030

1209 De Rosnay, P., Drusch, M., Vasiljevic, D., & others. (2013). A simplified extended Kalman
1210 filter for the global operational soil moisture analysis at ECMWF. *Quarterly Journal Of*.
1211 https://rmets.onlinelibrary.wiley.com/doi/abs/10.1002/qj.2023

1212 Dibia, E., R. Reichle, J. Anderson, and X.-Z. Liang (2023), Non-Gaussian Ensemble Filtering
1213 and Adaptive Inflation for Soil Moisture Data Assimilation, Journal of
1214 Hydrometeorology, 24, 1039-1053, doi:10.1175/JHM-D-22-0046.1

1215 Dong, J., & Crow, W. T. (2017). An Improved Triple Collocation Analysis Algorithm for
1216 Decomposing Autocorrelated and White Soil Moisture Retrieval Errors. *Journal of*
1217 *Geophysical Research: Atmospheres*, *122*(24), 13,081-13,094.
1218 https://doi.org/10.1002/2017JD027387

1219 Dong, J., Lei, F., & Crow, W. T. (2022). Land transpiration-evaporation partitioning errors
1220 responsible for modeled summertime warm bias in the central United States. *Nature*
1221 *Communications*, *13*(1), 336. https://doi.org/10.1038/s41467-021-27938-6

1222 Dong, J., Wei, L., Chen, X., Duan, Z., & Lu, Y. (2020). An instrument variable based
1223 algorithm for estimating cross-correlated hydrological remote sensing errors. *Journal of*
1224 *Hydrology*, *581*, 124413. https://doi.org/10.1016/j.jhydrol.2019.124413

1225 Dong, J., Crow, W. T., & Bindlish, R. (2018). The Error Structure of the SMAP Single and
1226 Dual Channel Soil Moisture Retrievals. *Geophys. Res. Lett.*, 2017GL075656.
1227 https://doi.org/10.1002/2017GL07565

1228 Dorigo, W. A., Scipal, K., Parinussa, R. M., Liu, Y. Y., Wagner, W., de Jeu, R. a. M., &
1229 Naeimi, V. (2010). Error characterisation of global active and passive microwave soil
1230 moisture datasets. *Hydrology and Earth System Sciences*, *14*(12), 2605–2616.
1231 https://doi.org/10.5194/hess-14-2605-2010

1232 Dorigo, W., Himmelbauer, I., Aberer, D., Schremmer, L., Petrakovic, I., Zappa, L.,
1233 Preimesberger, W., Xaver, A., Annor, F., Ardö, J., & Others. (2021). The International
1234 Soil Moisture Network: Serving Earth system science for over a decade. *Hydrol. Earth*
1235 *Syst. Sci. Discuss.*, 1–83. https://doi.org/10.5194/hess-25-5749-2021

1236 Draper, C. S., Reichle, R. H., De Lannoy, G. J. M., & Liu, Q. (2012). Assimilation of passive
1237 and active microwave soil moisture retrievals. *Geophys. Res. Lett.*, *39*(4), L04401.
1238 https://doi.org/10.1029/2011GL050655

1239 Entekhabi, D., Njoku, E. G., O'Neill, P. E., Kellogg, K. H., Crow, W. T., Edelstein, W. N.,
1240 Entin, J. K., Goodman, S. D., Jackson, T. J., Johnson, J., Kimball, J., Piepmeier, J. R.,
1241 Koster, R. D., Martin, N., McDonald, K. C., Moghaddam, M., Moran, S., Reichle, R.,
1242 Shi, J. C., … Zyl, J. V. (2010). The Soil Moisture Active Passive (SMAP) Mission. *Proc.*
1243 *IEEE*, *98*(5), 704–716. https://doi.org/10.1109/JPROC.2010.2043918

1244 Entekhabi, D., Reichle, R. H., Koster, R. D., & Crow, W. T. (2010). Performance Metrics for
1245 Soil Moisture Retrievals and Application Requirements. *Journal of Hydrometeorology*,
1246 *11*(3), 832–840. https://doi.org/10.1175/2010JHM1223.1

1247 Ford, T. W., & Quiring, S. M. (2019). Comparison of Contemporary In Situ, Model, and
1248 Satellite Remote Sensing Soil Moisture With a Focus on Drought Monitoring. *Water*
1249 *Resources Research*, *55*(2), 1565–1582. https://doi.org/10.1029/2018WR024039

1250 Gao, H., Wood, E. F., Jackson, T. J., Drusch, M., & Bindlish, R. (2006). *Using TRMM/TMI*
1251 *to Retrieve Surface Soil Moisture over the Southern United States from 1998 to 2002*.
1252 https://doi.org/10.1175/JHM473.1

1253 Gaspari, G., & Cohn, S. E. (1999). Construction of correlation functions in two and three
1254 dimensions. *Quart. J. Roy. Meteor. Soc.*, *125*(554), 723–757.
1255 https://doi.org/10.1002/qj.49712555417

1256 Gelaro, R., McCarty, W., Suárez, M. J., Todling, R., Molod, A., Takacs, L., Randles, C.,
1257 Darmenov, A., Bosilovich, M. G., Reichle, R., Wargan, K., Coy, L., Cullather, R.,
1258 Draper, C., Akella, S., Buchard, V., Conaty, A., da Silva, A., Gu, W., … Zhao, B. (2017).

1259 The Modern-Era Retrospective Analysis for Research and Applications, Version 2
1260 (MERRA-2). *J. Clim.*, *30*(Iss 13), 5419–5454. https://doi.org/10.1175/JCLI-D-16-0758.1

1261 Girotto, M., De Lannoy, G. J. M., Reichle, R. H., & Rodell, M. (2016). Assimilation of
1262 gridded terrestrial water storage observations from GRACE into a land surface model.
1263 *Water Resour. Res.*, *52*(5), 4164–4183. https://doi.org/10.1002/2015WR018417

1264 Gómez, B., Charlton-Pérez, C. L., Lewis, H., & Candy, B. (2020). The Met Office
1265 Operational Soil Moisture Analysis System. *Remote Sensing*, *12*(22), 3691.
1266 https://doi.org/10.3390/rs12223691

1267 Gruber, A., De Lannoy, G., Albergel, C., Al-Yaari, A., Brocca, L., Calvet, J.-C., Colliander,
1268 A., Cosh, M., Crow, W., Dorigo, W., Draper, C., Hirschi, M., Kerr, Y., Konings, A.,
1269 Lahoz, W., McColl, K., Montzka, C., Muñoz-Sabater, J., Peng, J., … Wagner, W. (2020).
1270 Validation practices for satellite soil moisture retrievals: What are (the) errors? *Remote*
1271 *Sens. Environ.*, *244*, 111806. https://doi.org/10.1016/j.rse.2020.111806

1272 Gruber, A., & Reichle, R. H. (2022). Uncertainty Estimation for SMAP Level-1 Brightness
1273 Temperature Assimilation at Different Timescales. *IEEE Journal of Selected Topics in*
1274 *Applied Earth Observations and Remote Sensing*, *15*, 9127–9145.
1275 https://doi.org/10.1109/JSTARS.2022.3216213

1276 Guo, Z., Dirmeyer, P. A., DelSole, T., & Koster, R. D. (2012). Rebound in Atmospheric
1277 Predictability and the Role of the Land Surface. *J. Clim.*, *25*(13), 4744–4749.
1278 https://doi.org/10.1175/JCLI-D-11-00651.1

1279 H SAF (2021a): ASCAT Surface Soil Moisture Climate Data Record v7 12.5 km sampling -
1280 Metop, EUMETSAT SAF on Support to Operational Hydrology and Water Management,
1281 DOI: 10.15770/EUM_SAF_H_0009. http://doi.org/10.15770/EUM_SAF_H_0009

1282 H SAF (2021b): ASCAT Surface Soil Moisture Climate Data Record v7 Extension 12.5 km
1283 sampling - Metop, EUMETSAT SAF on Support to Operational Hydrology and Water
1284 Management, DOI: 10.15770/EUM_SAF_H_0010.

1285 Humphrey, V., Berg, A., Ciais, P., Gentine, P., Jung, M., Reichstein, M., Seneviratne, S. I., &
1286 Frankenberg, C. (2021). Soil moisture–atmosphere feedback dominates land carbon
1287 uptake variability. *Nature*, *592*(7852), 65–69. https://doi.org/10.1038/s41586-021-03325-
1288 5

1289 Jackson, T. J., & Schmugge, T. J. (1991). Vegetation effects on the microwave emission of
1290 soils. *Remote Sensing of Environment*, *36*(3), 203–212. https://doi.org/10.1016/0034-
1291 4257(91)90057-D

1292 Kerr, Y. H., Waldteufel, P., Wigneron, J.-P., Delwart, S., Cabot, F., Boutin, J., Escorihuela,
1293 M.-J., Font, J., Reul, N., Gruhier, C., Juglea, S. E., Drinkwater, M. R., Hahne, A., Martín-
1294 Neira, M., & Mecklenburg, S. (2010). The SMOS Mission: New Tool for Monitoring
1295 Key Elements ofthe Global Water Cycle. *Proceedings of the IEEE*, *98*(5), 666–687.
1296 Proceedings of the IEEE. https://doi.org/10.1109/JPROC.2010.2043032

1297 Koster, R. D., Chang, Y., Wang, H., & Schubert, S. D. (2016). *Impacts of Local Soil*
1298 *Moisture Anomalies on the Atmospheric Circulation and on Remote Surface*
1299 *Meteorological Fields during Boreal Summer: A Comprehensive Analysis over North*
1300 *America*. https://doi.org/10.1175/JCLI-D-16-0192.1

1301 Koster, R. D., Dirmeyer, P. A., Guo, Z., Bonan, G., Chan, E., Cox, P., Gordon, C. T., Kanae,
1302 S., Kowalczyk, E., Lawrence, D., Liu, P., Lu, C.-H., Malyshev, S., McAvaney, B.,
1303 Mitchell, K., Mocko, D., Oki, T., Oleson, K., Pitman, A., … GLACE Team. (2004).
1304 Regions of strong coupling between soil moisture and precipitation. *Science*, *305*(5687),
1305 1138–1140. https://doi.org/10.1126/science.1100217

1306 Koster, R. D., Suarez, M. J., Ducharne, A., Stieglitz, M., & Kumar, P. (2000). A catchment-
1307 based approach to modeling land surface processes in a general circulation model: 1.
1308 Model structure. *J. Geophys. Res.*, *105*(D20), 24809–24822.
1309 https://doi.org/10.1029/2000JD900327

1310 Kumar, S., Dirmeyer, P. A., Peters-Lidard, C. D., Bindlish, R., & Bolten, J. (2018).
1311 Information theoretic evaluation of satellite soil moisture retrievals. *Remote Sensing of*
1312 *Environment*, *204*, 392–400. https://doi.org/10.1016/j.rse.2017.10.016

1313 Kumar, S., Kolassa, J., Reichle, R., Crow, W., de Lannoy, G., de Rosnay, P., MacBean, N.,
1314 Girotto, M., Fox, A., Quaife, T., Draper, C., Forman, B., Balsamao, G., Steele-Dunne, S.,
1315 Albergel, C., Bonan, B., Calvet, J.-C., Dong, J., Liddy, H., & Ruston, B. (2022). An
1316 agenda for land data assimilation priorities: Realizing the promise of terrestrial water,
1317 energy, and vegetation observations from space. *J. Adv. Model. Earth Syst.*
1318 https://doi.org/10.1029/2022ms003259

Kumar, S., Peters-Lidard, C., Tian, Y., Reichle, R., Geiger, J., Alonge, C., Eylander, J., & Houser, P. (2008). An integrated hydrologic modeling and data assimilation framework. *Computer*, *41*(12), 52–59. https://doi.org/10.1109/MC.2008.475

Lievens, H., Reichle, R. H., Liu, Q., De Lannoy, G. J. M., Dunbar, R. S., Kim, S. B., Das, N. N., Cosh, M., Walker, J. P., & Wagner, W. (2017). Joint Sentinel-1 and SMAP data assimilation to improve soil moisture estimates. *Geophys. Res. Lett.*, *44*(12), 6145–6153. https://doi.org/10.1002/2017GL073904

Lucchesi, R. (2013). *File Specification for GEOS-5 FP (Forward Processing)* (GSFC-E-DAA-TN19791; NASA Technical Report).

Mironov, V. L., Dobson, M. C., Kaupp, V. H., Komarov, S. A., & Kleshchenko, V. N. (2004). Generalized refractive mixing dielectric model for moist soils. *IEEE Transactions on Geoscience and Remote Sensing*, *42*(4), 773–785. IEEE Transactions on Geoscience and Remote Sensing. https://doi.org/10.1109/TGRS.2003.823288

Naeimi, V., Scipal, K., Bartalis, Z., Hasenauer, S., & Wagner, W. (2009). An Improved Soil Moisture Retrieval Algorithm for ERS and METOP Scatterometer Observations. *IEEE Trans. Geosci. Remote Sens.*, *47*(7), 1999–2013.

Njoku, E. G., Jackson, T. J., Lakshmi, V., Chan, T. K., & Nghiem, S. V. (2003). Soil moisture retrieval from AMSR-E. *IEEE Transactions on Geoscience and Remote Sensing*, *41*(2), 215–229. IEEE Transactions on Geoscience and Remote Sensing. https://doi.org/10.1109/TGRS.2002.808243

O'Neill, P. E., Chan, S., Njoku, E. G., Jackson, T., Bindlish, R., & Chaubell, M. J. (2021). *SMAP L3 Radiometer Global Daily 36 km EASE-Grid Soil Moisture, Version 8* [Dataset]. NASA National Snow and Ice Data Center Distributed Active Archive Center. https://doi.org/10.5067/OMHVSRGFX38O

Owe, M., de Jeu, R., & Holmes, T. (2008). Multisensor historical climatology of satellite-derived global land surface moisture. *Journal of Geophysical Research: Earth Surface*, *113*(F1). https://doi.org/10.1029/2007JF000769

Pablos, M., González-Zamora, Á., Sánchez, N., & Martínez-Fernández, J. (2018). Assessment of Root Zone Soil Moisture Estimations from SMAP, SMOS and MODIS Observations. *Remote Sensing*, *10*(7), Article 7. https://doi.org/10.3390/rs10070981

1349 Parinussa, R. M., Holmes, T. R. H., Wanders, N., Dorigo, W. A., & Jeu, R. A. M. de. (2015).
1350 *A Preliminary Study toward Consistent Soil Moisture from AMSR2*.
1351 https://doi.org/10.1175/JHM-D-13-0200.1

1352 Qiu, J., Dong, J., Crow, W. T., Zhang, X., Reichle, R. H., & De Lannoy, G. J. M. (2021). The
1353 benefit of brightness temperature assimilation for the SMAP Level-4 surface and root-
1354 zone soil moisture analysis. *Hydrology and Earth System Sciences*, *25*(3), 1569–1586.
1355 https://doi.org/10.5194/hess-25-1569-2021

1356 Reichle, R. H. (2008). Data assimilation methods in the Earth sciences. *Adv. Water Resour.*,
1357 *31*(11), 1411–1418. https://doi.org/10.1016/j.advwatres.2008.01.001

1358 Reichle, R. H., Crow, W. T., & Keppenne, C. L. (2008). An adaptive ensemble Kalman filter
1359 for soil moisture data assimilation. *Water Resour. Res.*, *44*(3), W03423.

1360 Reichle, R. H., De Lannoy, G. J. M., Liu, Q., Ardizzone, J. V., Colliander, A., Conaty, A.,
1361 Crow, W., Jackson, T. J., Jones, L. A., Kimball, J. S., Koster, R. D., Mahanama, S. P.,
1362 Smith, E. B., Berg, A., Bircher, S., Bosch, D., Caldwell, T. G., Cosh, M., González-
1363 Zamora, Á., … Zeng, Y. (2017). Assessment of the SMAP Level-4 Surface and Root-
1364 Zone Soil Moisture Product Using In Situ Measurements. *J. Hydrometeorol.*, *18*(10),
1365 2621–2645. https://doi.org/10.1175/JHM-D-17-0063.1

1366 Reichle, R. H., De Lannoy, G. J. M., Liu, Q., Koster, R. D., Kimball, J. S., Crow, W. T.,
1367 Ardizzone, J. V., Chakraborty, P., Collins, D. W., Conaty, A. L., Girotto, M., Jones, L.
1368 A., Kolassa, J., Lievens, H., Lucchesi, R. A., & Smith, E. B. (2017). Global Assessment
1369 of the SMAP Level-4 Surface and Root-Zone Soil Moisture Product Using Assimilation
1370 Diagnostics. *J. Hydrometeorol.*, *18*(12), 3217–3237. https://doi.org/10.1175/JHM-D-17-
1371 0130.1

1372 Reichle, R. H., Kumar, S. V., Mahanama, S. P. P., Koster, R. D., & Liu, Q. (2010).
1373 Assimilation of Satellite-Derived Skin Temperature Observations into Land Surface
1374 Models. *J. Hydrometeorol.*, *11*(5), 1103–1122.

1375 Reichle, R. H., Liu, Q., & Ardizzone, J. V. (2023). *Soil Moisture Active Passive (SMAP)*
1376 *Project Assessment Report for Version 7 of the L4_SM Data Product* (NASA/TM–2023–
1377 104606/Vol. 64; Technical Report Series on Global Modeling and Data Assimilation,
1378 Volume 64).

Reichle, R. H., Liu, Q., Ardizzone, J. V., Crow, W. T., De Lannoy, G. J. M., Dong, J., Kimball, J. S., & Koster, R. D. (2021). The Contributions of Gauge-Based Precipitation and SMAP Brightness Temperature Observations to the Skill of the SMAP Level-4 Soil Moisture Product. *J. Hydrometeorol.*, *22*(2), 405–424. https://doi.org/10.1175/JHM-D-20-0217.1

Reichle, R. H., Liu, Q., Ardizzone, J. V., Crow, W. T., De Lannoy, G. J. M., Kimball, J. S., & Koster, R. D. (2023). IMERG Precipitation Improves the SMAP Level-4 Soil Moisture Product. *J. Hydrometeorol.*, *24*(10), 1699–1723. https://doi.org/10.1175/JHM-D-23-0063.1

Reichle, R. H., Liu, Q., Koster, R. D., Crow, W. T., De Lannoy, G. J. M., Kimball, J. S., Ardizzone, J. V., Bosch, D., Colliander, A., Cosh, M., Kolassa, J., Mahanama, S. P., Prueger, J., Starks, P., & Walker, J. P. (2019). Version 4 of the SMAP level-4 soil moisture algorithm and data product. *J. Adv. Model. Earth Syst.*, *11*(10), 3106–3130. https://doi.org/10.1029/2019ms001729

Reichle, R. H., McLaughlin, D. B., & Entekhabi, D. (2002). Hydrologic Data Assimilation with the Ensemble Kalman Filter. *Mon. Weather Rev.*, *130*(1), 103–114. https://doi.org/10.1175/1520-0493(2002)130<0103:HDAWTE>2.0.CO;2

Reichle, R. H., Zhang, S. Q., Kolassa, J., Liu, Q., & Todling, R. (2023). A weakly coupled land surface analysis with SMAP radiance assimilation improves GEOS medium-range forecasts of near-surface air temperature and humidity. *Quarterly Journal of the Royal Meteorological Society*, *149*(754), 1867–1889. https://doi.org/10.1002/qj.4486

Reichle, R. H., Zhang, S. Q., Liu, Q., Draper, C. S., Kolassa, J., & Todling, R. (2021). Assimilation of SMAP Brightness Temperature Observations in the GEOS Land-Atmosphere Data Assimilation System. *IEEE J Sel Top Appl Earth Obs Remote Sens*, *14*, 10628–10643. https://doi.org/10.1109/jstars.2021.3118595

Santanello, J. A., Dirmeyer, P. A., Ferguson, C. R., Findell, K. L., Tawfik, A. B., Berg, A., Ek, M., Gentine, P., Guillod, B. P., van Heerwaarden, C., Roundy, J., & Wulfmeyer, V. (2018). Land–Atmosphere Interactions: The LoCo Perspective. *Bull. Am. Meteorol. Soc.*, *99*(6), 1253–1272. https://doi.org/10.1175/BAMS-D-17-0001.1

1408 Schmugge, T., Gloersen, P., Wilheit, T., & Geiger, F. (1974). Remote sensing of soil
1409 moisture with microwave radiometers. *Journal of Geophysical Research (1896-1977)*,
1410 *79*(2), 317–323. https://doi.org/10.1029/JB079i002p00317

1411 Seneviratne, S. I., Corti, T., Davin, E. L., Hirschi, M., Jaeger, E. B., Lehner, I., Orlowsky, B.,
1412 & Teuling, A. J. (2010). Investigating soil moisture–climate interactions in a changing
1413 climate: A review. *Earth-Sci. Rev.*, *99*(3), 125–161.
1414 https://doi.org/10.1016/j.earscirev.2010.02.004

1415 Seo, E., Lee, M.-I., & Reichle, R. H. (2021). Assimilation of SMAP and ASCAT soil
1416 moisture retrievals into the JULES land surface model using the Local Ensemble
1417 Transform Kalman Filter. *Remote Sens. Environ.*, *253*, 112222.
1418 https://doi.org/10.1016/j.rse.2020.112222

1419 Stillman, S., & Zeng, X. (2018). Evaluation of SMAP Soil Moisture Relative to Five Other
1420 Satellite Products Using the Climate Reference Network Measurements Over USA. *IEEE*
1421 *Transactions on Geoscience and Remote Sensing*, *56*(11), 6296–6305. IEEE Transactions
1422 on Geoscience and Remote Sensing. https://doi.org/10.1109/TGRS.2018.2835316

1423 Su, C.-H., Ryu, D., Crow, W. T., & Western, A. W. (2014). Beyond triple collocation:
1424 Applications to soil moisture monitoring. *Journal of Geophysical Research:*
1425 *Atmospheres*, *119*(11), 6419–6439. https://doi.org/10.1002/2013JD021043

1426 Wagner, W., Hahn, S., Kidd, R., Melzer, T., Bartalis, Z., Hasenauer, S., Figa-Saldaña, J., de
1427 Rosnay, P., Jann, A., Schneider, S., Komma, J., Kubu, G., Brugger, K., Aubrecht, C.,
1428 Züger, J., Gangkofner, U., Kienberger, S., Brocca, L., Wang, Y., … Steinnocher, K.
1429 (2013). The ASCAT soil moisture product: A review of its specifications, validation
1430 results, and emerging applications. *Meteorol. Z.*, *22*(1), 5–33.
1431 https://doi.org/10.1127/0941-2948/2013/0399

1432 Wagner, W., Lemoine, G., & Rott, H. (1999). A Method for Estimating Soil Moisture from
1433 ERS Scatterometer and Soil Data. *Remote Sensing of Environment*, *70*(2), 191–207.
1434 https://doi.org/10.1016/S0034-4257(99)00036-X

1435 Wagner, W., Lindorfer, R., Hahn, S., Kim, H., Vreugdenhil, M., Gruber, A., Fischer, M., &
1436 Trnka, M. (2024). Global Scale Mapping of Subsurface Scattering Signals Impacting
1437 ASCAT Soil Moisture Retrievals. *IEEE Transactions on Geoscience and Remote*

Sensing, 1–1. IEEE Transactions on Geoscience and Remote Sensing. https://doi.org/10.1109/TGRS.2024.3429550

Wooldridge, J. M. (2024). Introductory econometrics: A modern approach (8th ed.). Cengage Learning, Inc.

Zhao, L., Yang, Z.-L., & Hoar, T. J. (2016). Global Soil Moisture Estimation by Assimilating AMSR-E Brightness Temperatures in a Coupled CLM4–RTM–DART System. *J. Hydrometeorol.*, *17*(9), 2431–2454. https://doi.org/10.1175/JHM-D-15-0218.1

Zhou, S., Park Williams, A., Lintner, B. R., Berg, A. M., Zhang, Y., Keenan, T. F., Cook, B. I., Hagemann, S., Seneviratne, S. I., & Gentine, P. (2021). Soil moisture–atmosphere feedbacks mitigate declining water availability in drylands. *Nat. Clim. Chang.*, 1–7. https://doi.org/10.1038/s41558-020-00945-z